Alto, California, USA) equipped with a 18.3 cm horizontal-bore 7.05 Tesla superconducting magnet (Oxford Instruments, UK).[21 22] To minimise bulk motion artefacts, data acquisitions were gated to respiration using a home-made mechanical switch activated by the ventilator piston at inspiration. This gating apparatus synchronised the rat respiration and the start of pulse sequence. The rats were anaesthetised, tracheotomised and ventilated with 800 ms/respiration cycle (figure 1A).

MR images were obtained using a spin-echo (SE) sequence. Repetition time (TR) was determined by the respiration rate and the number of multislice, and was 4800 ms (=800 ms×6 slices). Unenhanced MR images of the liver were first obtained, and then MRI was performed 15 min after the injection of SPIO (10 μmol Fe/kg body weight or 50 μmol Fe/kg body weight) via the left external jugular vein.

SI values of the liver parenchyma in the region of interest (over 100 pixels) were normalised to the standard deviation of background noise and expressed as signal-to-noise ratio. SI of the whole liver was measured on each MR image, and the relative signal enhancement (RSE) of the rat liver was calculated using the following equation: RSE (%)=SIpost/SIpre×100, where SIpre and SIpost are the signal intensities of the whole liver parenchyma before and after injection of SPIO respectively.[16]

Evaluation of accumulation of fluorescent microspheric beads in rat livers

Rats fed an MCD diet (n=6) and control rats (n=6) or Zucker *fa/fa* rats (n=4) were deeply anaesthetised with pentobarbital sodium (25–50 mg/kg, Nembutal; Abbott Laboratories) administered intraperitoneally, and Fluoresbrite YG carboxylate microspheres 2.00 μm (2.5% slide-latex, Polyscience, Warrington, Pennsylvania, USA) were injected via a left external jugular vein catheter. One hour after injection, the animals were re-anaesthetised, and their livers removed. The number of accumulated microspheres in 10 high-power fields was counted by fluorescent microscopy.

Kupffer cells in liver sections

Liver sections were stained for the presence of KCs with ED2 monoclonal antibody (BMA Biomedicals AG, Switzerland).[23] The number of KCs per field area of digital photomicrographs was quantified with a computerised image analysis system (Macintosh MacSCOPE version 2.591).[18]

Patients

Twenty-six patients (14 women/12 men) with elevated transaminases and a diagnosis of NAFLD on abdominal ultrasonography, and 10 patients with chronic hepatitis C (five women/five men) and four healthy volunteers as controls, participated in this study. Patients with known use of methotrexate, tamoxifen, corticoids, insulin or alcohol in excess of 20 g per day and patients with other known causes of liver disease, including viral hepatitis, haemochromatosis, Wilson disease and autoimmune liver diseases, were excluded from this study. Informed consent was obtained for SPIO-MRI, abdominal CT, liver biopsy or laboratory tests. Twenty-six patients with NAFLD consented to an abdominal CT scan to quantify the degree of hepatic steatosis, defined as a liver/spleen ratio (L/S ratio): <0.9 moderate to severe hepatic steatosis and ≥0.9 mild hepatic steatosis.[24] Liver biopsies were also performed in 20 patients with NAFLD: 13 (seven women/men men) of these fulfilled criteria diagnostic for NASH.[25]

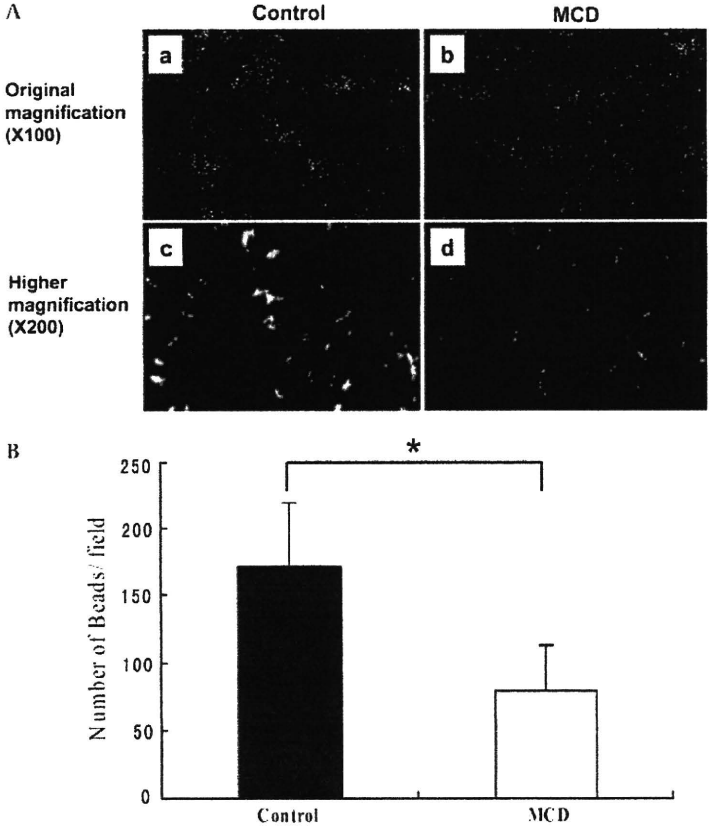

Figure 2 Uptake of fluorescent microspheric beads by Kupffer cells. (A) Uptake of microbeads in a liver section as judged by fluorescent microscopy. Fluorescent microbeads formed large aggregates in control livers, whereas the beads were disseminated in the livers of rats fed a methionine-choline deficient (MCD) diet. (B) The number of fluorescent microbeads taken up in liver sections of control and rats fed an MCD diet. The number of fluorescent beads in livers of rats fed an MCD diet was fewer than that in control rat livers (171.33±48.37/field in control rats (n=6), 78.63±34.8/field in rats fed an MCD diet (n=6), *p<0.005). ■, control rats; □, rats fed an MCD diet.

Gut 2010;**59**:258–266. doi:10.1136/gut.2009.176651

Patient MRI

MRI examinations were performed on a 1.5 T MRI system (Signa Horizon, GE Medical Systems, USA) using a body phased array coil. Unenhanced T1- and T2-weighted images of the whole liver were obtained as routine. SPIO (8 μmol Fe/kg body weight) was injected via the antecubital vein. Fast imaging was performed using the SPGR (spoiled gradient recalled acquisition in the steady state) technique at 200/20/20 degree (TR/TE/flip angle) in suspended respiration to analyse the uptake of SPIO by the liver. Whole-liver images were acquired within 15 s.

The parameters used were field of view, 320×320 mm; slice thickness, 7.0 mm; interslice gap, 3.0 mm, phase×frequency matrix, 128×256; and number of acquisitions, one. SPGR imaging was repeated at multiple time points (pre-contrast, 40 s, 2, 3, 5, 10, 15, 20, 25 and 30 min after injection of SPIO). The RSE was calculated as above.

Histological examination

Haematoxylin and eosin stained liver biopsy specimens of patients with NAFLD were scored according to the NASH Clinical Research Network Scoring System[24] by two pathologists blinded to the patients' clinical data. An NAFLD Activity Score (NAS) of ≥5 was classified as NASH and ≥3 as non-NASH.[25]

KCs in patients' liver biopsy specimens

KCs in liver biopsy specimens were detected by staining with anti-CD68 (KP-1, DAKO)[18] and quantified as above.[18]

Statistical analysis

Results are presented as mean±SD for continuous data or as numbers for categorical data. A univariate analysis was conducted using the Mann–Whitney U test to assess the significance between the two groups based on the quantitative data. Qualitative data were compared using Fisher's exact test. Spearman's coefficient of correlation was used to evaluate the relationship between the two groups. Statistical significance was accepted at $p<0.05$. All analyses were performed using Stat View.

RESULTS

Rats with experimentally induced NASH have reduced KC uptake function

Figure 1B shows representative MR images of rats fed a control or MCD diet with and without infusion of SPIO. Images were scarcely affected by motion artefact (a). In the absence of SPIO, livers of rats fed an MCD diet (d) had a higher SI than control rats (a). After SPIO (10 μmol Fe/kg), SI in control livers dramatically decreased (b), whereas little signal reduction was seen in livers of rats fed an MCD diet (e). Similarly, after 50 μmol Fe/kg SPIO, the SI of the control livers almost disappeared (c), with minimal signal reduction in MCD-fed rats (f).

Figure 1C shows quantitatively the changes in SI in control or MCD-fed rats, depicted qualitatively in figure 1B above. Signal intensities were standardised using the SI of water as an external standard. At baseline there was a statistically significant difference between the SI of control and MCD-fed rats (0.22±0.04 vs 0.44±0.09, $p<0.01$). After infusion of 10 and 50 μmol Fe/kg

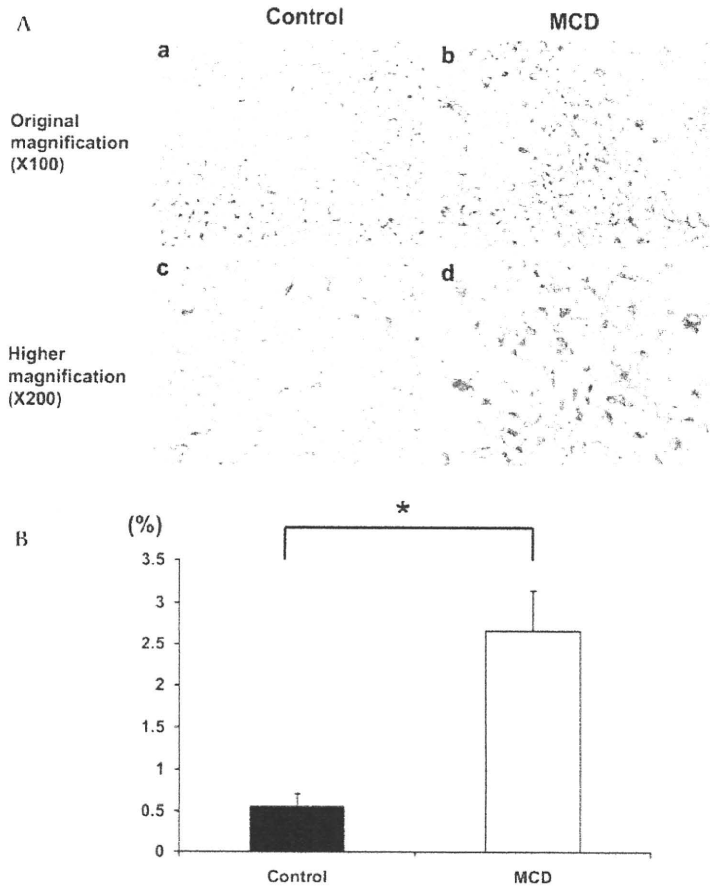

Figure 3 The number of Kupffer cells (KCs) in the livers of rats fed a methionine-choline deficient (MCD) diet. (A) Immunostaining of KCs in liver sections. The number of KCs in the livers of rats fed an MCD diet was increased compared with that of controls. (B) The area occupied by KCs cells estimated by image analysis in the livers of rats fed an MCD diet (2.6675±0.4795%, n=6) is clearly shown to be increased compared with that of control rats (0.5606±0.1541%, n=6, *$p<0.0001$). ■, control rats; □, rats fed an MCD diet.

SPIO, this difference was accentuated and a greater SI reduction was seen in controls than in MCD-fed rats (0.13±0.03 vs 0.42±0.08 at 10 μmol Fe/kg SPIO and 0.069±0.009 vs 0.337±0.063 at 50 μmol Fe/kg SPIO, p<0.01), with minimal change of SI in the MCD-fed at each SPIO dose.

To more accurately compare the uptake function of KCs observed with an MCD diet, SIs were calculated as the RSE (figure 1D), with the RSE at baseline set at 100%. After infusion of SPIO (10 μmol Fe/kg), a substantial reduction of SI was observed in controls (RSE=100% vs 58.0±2.0%, p<0.05), whereas there was no significant reduction in RSE in rats fed an MCD diet (RSE=100% versus 95.4±4.7%, p>0.05). With infusion of SPIO at 50 μmol Fe/kg a more marked reduction in RSE, than was seen at 10 μmol Fe/kg, was found with controls (100% vs 32.5±3.6%, p<0.05) compared with rats fed an MCD diet (100% vs 77.3±3.7%, p<0.05). Furthermore, there was a clear and statistically significant difference (p<0.05) in RSE between control rats and rats fed an MCD diet at either of the SPIO concentrations, with the RSE of the rats fed an MCD diet being consistently higher than controls (95.4±4.7% vs 58.0±2.0%) at SPIO 10 μmol Fe/kg, and (77.3±3.7% vs 32.5±3.6%) at SPIO 50 μmol Fe/kg. Therefore, uptake function of KCs in rats fed an MCD diet is impaired compared with that in control rats.

Similarly, as shown in online supplementary figure 1, the RSE of SPIO-MRI in Zucker *fa/fa* rats was significantly higher than that of their lean littermates (59.5±12.5% vs 47.2±11.7% at SPIO 10 μmol Fe/kg, p<0.05, and 27.0±9.8% vs 18.2±9.0% at SPIO 50 μmol Fe/kg, p<0.05) indicating that KC uptake function in the livers of obese, insulin-resistant, steatotic Zucker *fa/fa* is impaired compared with that of controls and so validating the results with the rats fed an MCD diet as above.

Uptake of fluorescent beads by KCs is reduced in experimental NASH

To confirm this suggested impairment of KC uptake function in our experimental models of NASH, fluorescent microspheric beads were now infused into the rats fed an MCD diet and Zucker *fa/fa* rats and the number of fluorescent beads in their livers enumerated to reflect clearance function of KCs.[13] Qualitatively, figure 2A shows that the fluorescent microspheric beads in the livers of rats fed an MCD diet were fewer (figure 2A, b and d) than in controls (figure 2A, a and c). Furthermore, the beads formed large aggregates in control livers (figure 2A, a and c), whereas they were disseminated in the MCD-fed rats liver (figure 2A, b and d). Quantitatively, there were fewer fluorescent beads in the livers of rats fed an MCD diet than in controls (171.33±48.37/field (n=6), controls vs 78.63±34.8/field (n=6), rats fed an MCD diet, p=0.003, figure 2B).

We also examined the correlation between the extent of hepatic steatosis and KC uptake function, and between NASH activity and KC uptake function in MCD-fed rats. Online supplementary figure 2 shows that the number of phagocytosed microbeads in the livers of rats fed an MCD diet after 12 weeks (78.63±34.81/field) was no different from that after 4 weeks of the MCD diet (75.15±6.69/field, p=0.873). The extent of steatosis was similar between rats at 12 weeks and 4 weeks, although the extent of hepatic fibrosis and inflammation were more severe at 12 weeks than at 4 weeks. Furthermore, the number of microbeads taken up after 2 weeks of the MCD diet (non-NASH with mild steatosis, 131.02±22.75/field) was higher than that at 4 weeks (severe hepatic steatosis, 75.15±6.69/field, p<0.01). These data suggests that KC uptake function in rats is not influenced by NASH activity or severity but rather by the extent of hepatic steatosis.

As with the rats fed an MCD diet, accumulation of fluorescent microbeads in the livers of steatotic Zucker *fa/fa* rats (online supplementary figure 3A) was significantly lower than that of their lean littermates (173.94±10.84/field vs 221.01±11.11/field, n=4, p<0.005; online supplementary figure 3B). Thus, the uptake function of KCs is reduced in experimental NASH.

KCs numbers in livers of rats fed an MCD diet are increased compared with controls

We next evaluated the number of KCs in the livers of rats fed an MCD diet by immunohistochemical staining with ED2 monoclonal antibody without infusion of fluorescent beads. The number of KCs in the livers of rats fed an MCD diet was significantly increased compared with control livers (figure 3A, a–d). In addition, the morphological appearance of the KCs was altered and they appear enlarged in the livers of MCD-fed rats (figure 3A, c and d). To quantity the number of KCs, the area occupied by KCs was estimated by image analysis. The area occupied by KCs in the livers of rats fed an MCD diet was clearly increased compared with that of control rats (2.6675±0.4795% (n=6) vs 0.5606±0.1541% (n=6), p<0.0001, figure 3B). Therefore, the impairment of KC uptake function in the MCD model of NAFLD is functional and is not due to a reduction in the numbers of KCs.

SPIO-MRI in patients with NAFLD

KC uptake function is impaired in patients with NAFLD

To determine the applicability of these animal studies to NAFLD, we now evaluated, using SPIO-MRI, the uptake function of KCs in the livers of patients with NAFLD and chronic hepatitis C (CH-C) as controls. The clinical characteristics of the CH-C and NAFLD groups are shown in table 1. Patients with NAFLD were younger and had higher body mass indices, calculated as weight (kg) divided by height (m) squared, than those with CH-C.

Table 1 Comparison of clinical characteristics of patients with chronic hepatitis C (CH-C) and non-alcoholic fatty liver disease (NAFLD)

	CH-C (n=10)	NAFLD (n=26)	p Value
Female/male	5/5	14/12	0.842
Age (years)	61.4±9.88	48.2±17.5	<0.05
BMI (kg/m^2)	22.9±2.7	31.1±6.8	<0.01
RBC (×10^4/μl)	428.0±40.1	464.4±50.3	<0.05
Ht (%)	40.0±3.8	42.6±4.2	0.099
Plt (×10^4/μl)	19.5±8.4	21.2±6.1	0.422
WBC (×10^3/μl)	4.724±1.321	6.260±1.967	<0.05
ALT (U/l)	41.6±22.3	82.2±62.2	0.056
AST (U/l)	40.3±17.4	55±35.0	0.184
LDH (U/l)	185.1±26.0	214.2±54.7	0.124
ALP (U/l)	255.6±88.5	227.9±56.8	0.209
γ-GTP (U/l)	28.1±13.4	60.8±36.2	<0.05
T-Bil (mg/dl)	0.58±0.24	0.84±0.32	<0.05
TP (g/dl)	7.76±0.37	7.39±0.47	<0.05
Alb (g/dl)	4.29±0.13	4.44±0.29	0.089
PT (%)	82.0±9.2	87.5±11.6	0.104
T-cho (mg/dl)	173.4±37.9	192.0±35.4	0.177
TG (mg/dl)	135.3±61.3	160.1±72.6	0.572
FPG (mg/dl)	101.4±11.9	108.8±34.9	0.498

Patients with NAFLD were younger and had higher BMI than those with CH-C (p<0.05). Alb, albumin; ALP, alkaline phosphatase; ALT, alanine transaminase; AST, aspartate aminotransferase; BMI, body mass index; FPG, fasting plasma glucose; Ht, haematocrit; γ-GTP, γ-glutamyltransferase; LDH, lactate dehydrogenase; Plt, platelets; PT, ????; RBC, red blood cells; T-Bil, total bilirubin; T-cho, total cholesterol; TG, triglycerides; TP, ????; WBC, white blood cells.

Gut 2010;**59**:258–266. doi:10.1136/gut.2009.176651

The liver MRI images before and after SPIO in patients with CH-C or NAFLD are shown in figure 4A. As shown, the SI of the liver images in CH-C decreased within 15 min after injection of SPIO. However, only a slight reduction of SI was seen in livers with NAFLD. We next compared the RSE in patients with CH-C and NAFLD. As shown, figure 4B, RSE in NAFLD was significantly higher than in controls (20.87±6.23% (n=26) vs 10.13±1.31% (n=10), p<0.0001), indicating that KC uptake function is impaired in NAFLD. Furthermore, we also studied SPIO-RSE in healthy volunteers (n=4). The RSE of healthy volunteers was almost the same as that of patients with CH-C (online supplementary figure 4B), but was demonstrably lower than that of patients with NAFLD (online supplementary figure 4A, p=0.0011).

KC uptake function in NAFLD worsens with the degree of hepatic steatosis

We next evaluated the relationship between RSE and degree of hepatic steatosis determined on abdominal CT. The RSE in patients with NAFLD with mild hepatic steatosis was significantly lower than in patients with moderate to severe hepatic steatosis (16.77±4.44% (n=8) vs 23.77±6.29% (n=14), p<0.05, figure 4C). Since the RSE is inversely proportional to KC function—that is, the larger the RSE, the worse the KC function, these results suggest therefore that KC uptake function worsens with the degree of hepatic steatosis in NAFLD.

We now sought to determine if KC uptake function was also related to the degree of steatosis on biopsy. We observed a strong positive correlation between the degree of hepatic steatosis and RSE on SPIO-MRI in the livers of patients with NAFLD (figure 4D, r=0.757, p<0.0005, n=20), confirming that the degree of KC uptake dysfunction in NAFLD is related to the extent of hepatic steatosis.

We also determined if age might have influenced the RSE on SPIO-MRI in our study. As shown in our online supplementary figure 5A, there was no significant correlation between age and RSE in the CH-C cohort. However, there was a significant correlation between age and RSE in patients with NAFLD

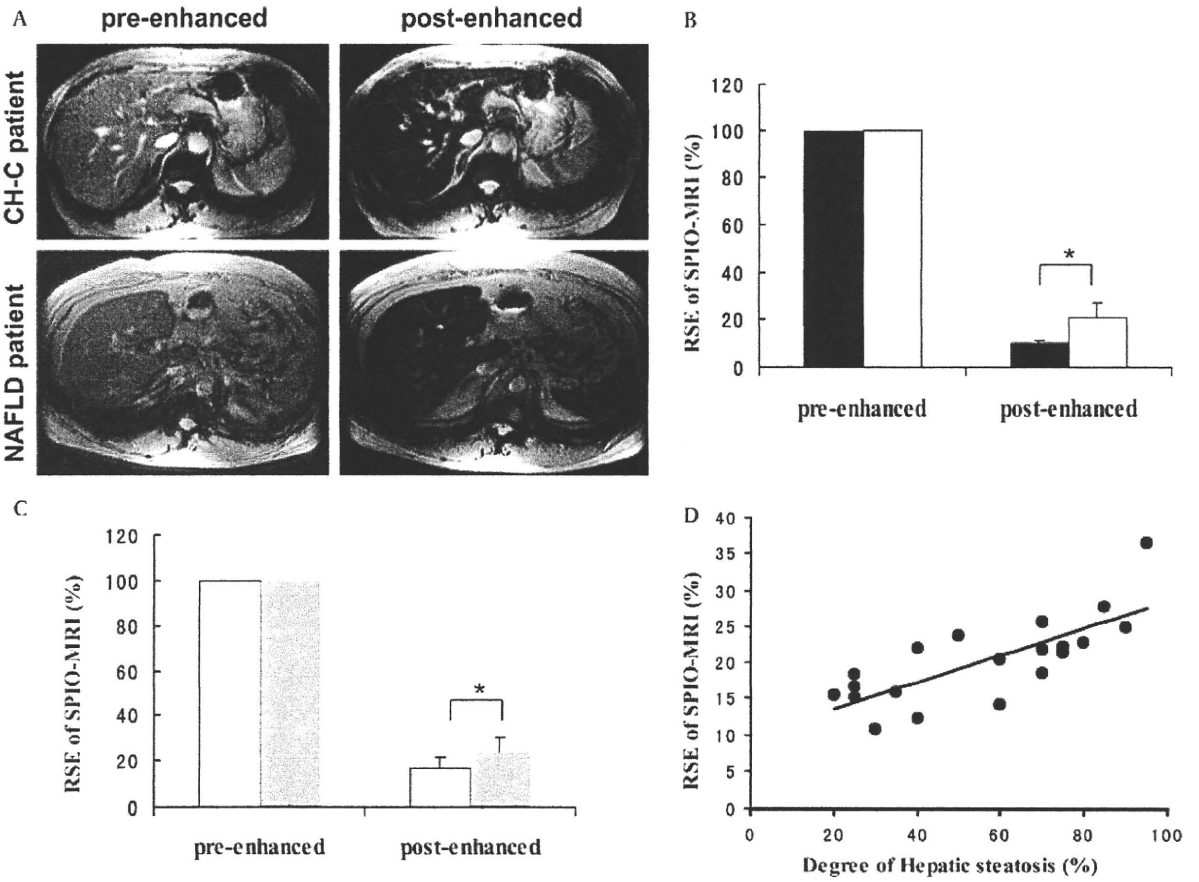

Figure 4 Super-paramagnetic iron oxide (SPIO)-MRI in patients with non-alcoholic fatty liver disease (NAFLD). (A) Representative MRI images of a patient with NAFLD and another with chronic hepatitis C (CH-C), pre-enhancement and post-enhancement with SPIO. (B) The relative signal enhancement (RSE) of the livers of patients with NAFLD and CH-C controls. RSE in the NAFLD group was statistically higher than in the CH-C control group (20.87±6.23% (n=26) vs 10.13±1.31% (n=10), *p<0.0001). ■, CH-C; □, NAFLD. (C) Relationship between the RSE and the degree of hepatic steatosis on abdominal CT. The RSE of patients with NAFLD who had mild hepatic steatosis was remarkably lower than that in patients with NAFLD who had moderate to severe hepatic steatosis (16.77±4.44% (n=8) vs 23.77±6.29% (n=14), *p<0.05). □, NAFLD with mild hepatic steatosis; , NAFLD with moderate to severe hepatic steatosis. (D) Relationship between degree of hepatic steatosis and RSE of SPIO-MRI in patients with NAFLD. A strong positive correlation was observed between the degree of hepatic steatosis and the RSE on SPIO-MRI in the livers of patients with NAFLD (r=0.757, p<0.0005, n=20).

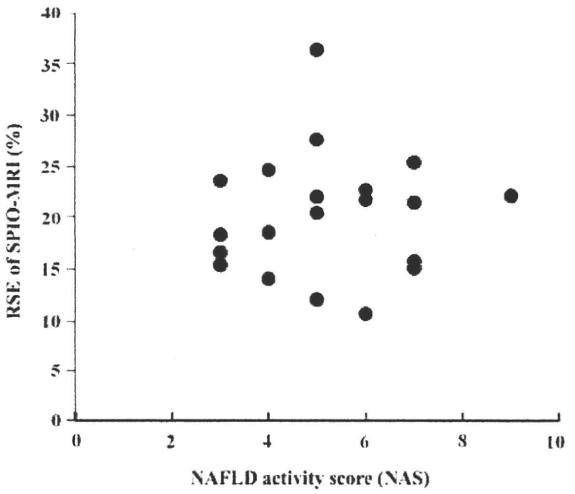

Figure 5 The relationship between non-alcoholic fatty liver disease (NAFLD) activity score (NAS) and relative signal enhancement (RSE) in patients with NAFLD. With NAS, 13 patients out of 20 were diagnosed as having the non-alcoholic steatohepatitis stage of NAFLD. The RSE of super-paramagnetic iron oxide (SPIO)-MRI in the 20 patients with NAFLD was not correlated with NAS ($r=0.0682$, $p=0.8072$, $n=20$).

(online supplementary figure 5B). In addition, the younger patients with NAFLD had more severe hepatic steatosis than the older patients in our study (online supplementary figure 5C). Therefore, RSE in NAFLD patients is influenced not by age but by the degree of hepatic steatosis.

KC uptake function is not related to NAFLD activity score

To now determine the relationship between the severity of NAFLD, as judged by the NAS and RSE, liver biopsies were scored according to the NASH Clinical Research Network Scoring System.[25] Accordingly, 13 of the 20 patients with NAFLD were classified as having NASH. The NAS was then correlated with RSE. As shown in figure 5, there was no correlation between the RSE and NAS, suggesting that KC uptake function may not be related to histological severity of NAFLD.

Reduced KC uptake function in NAFLD is not dependent on a reduction on the number of KCs

As with the rat studies, we now sought to determine if the apparent KC dysfunction in NAFLD was secondary to a lowering of the number of KCs. To this end we stained for the presence of KCs by immunohistochemistry and quantified the numbers by image analysis. There was no correlation ($p>0.05$) between the severity of steatosis and number of KCs, nor between the number of KCs and RSE (figure 6A–C). Therefore, the observed reduction in KC uptake function in NAFLD is not dependent on a reduction in KC numbers.

Reduced KC uptake function in NAFLD is not dependent on reduced hepatic blood flow

It is plausible that the changes in RSE in patients with NAFLD and CH-C were due to changes in the liver's microcirculation since fat accumulation in hepatocytes is associated with increases in hepatocyte cell volume which may compromise the hepatic sinusoidal space.[26] To ensure that changes in RSE in patients with NAFLD and CH-C were not due to changes in microcirculatory blood flow, we therefore compared the change in RSE with, time after injection of SPIO, in both patient groups. RSE gradually decreased in both groups after injection of SPIO and had reached a plateau by 15 min (figure 7). Consequently, differences at 15 min were reasonably chosen as standard in all the human studies above and observed differences between the NAFLD and control groups are unlikely, therefore, to be the result of changes in the microcirculation.

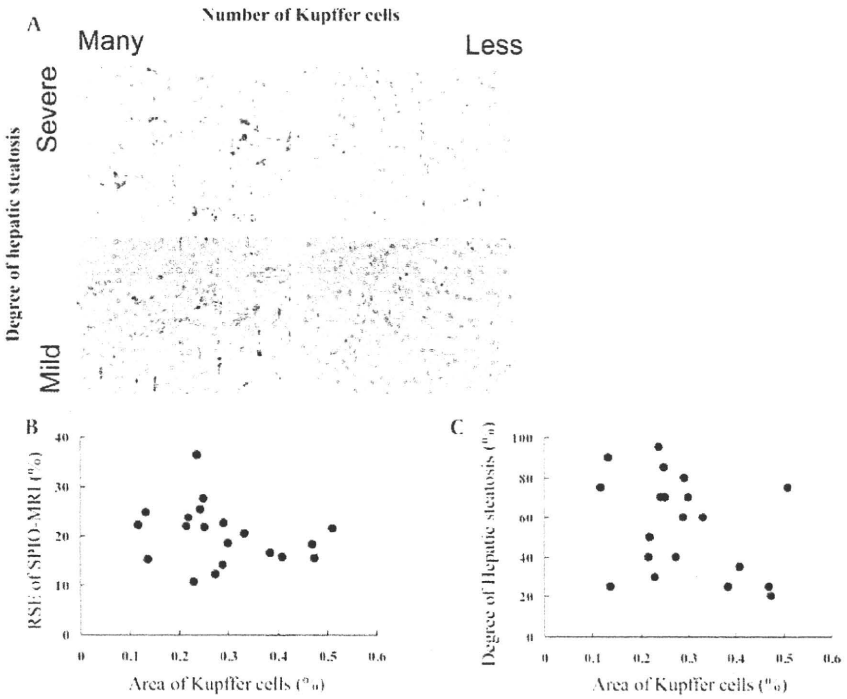

Figure 6 The number of Kupffer cells (KCs), degree of hepatic steatosis and relative signal enhancement (RSE) in patients with non-alcoholic fatty liver disease (NAFLD). (A) Four typical histological patterns based on the degree of fatty droplets and the number of KCs in the liver of patients with NAFLD. (B) The relationship between the area occupied by KCs estimated by image analysis and the RSE on super-paramagnetic iron oxide (SPIO)-MRI in patients with NAFLD. There was no correlation between these parameters ($r=-0.252$, $p=0.287$, $n=20$). (C) The relationship between the degree of hepatic steatosis and the area occupied by KCs in the livers of patients with NAFLD. No correlation between the degree of hepatic steatosis and the number of KCs was seen ($r=-0.345$, $p=0.141$, $n=20$).

Gut 2010;**59**:258–266. doi:10.1136/gut.2009.176651

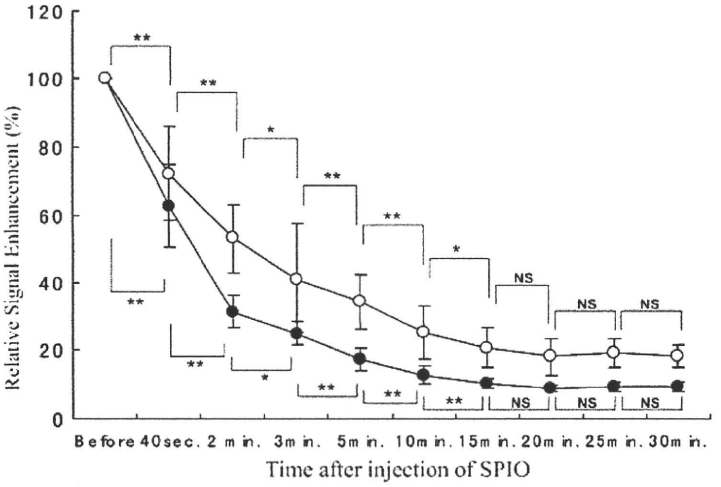

Figure 7 Changes in relative signal enhancement (RSE) in patients with non-alcoholic fatty liver disease (NAFLD) and chronic hepatitis C (CH-C) with time after injection of super-paramagnetic iron oxide (SPIO). RSE gradually decreased in both groups after injection of SPIO and had reached a plateau by 15 min (●, CH-C: n=10, ○, NAFLD, n=26, *p<0.05, **p<0.01).

DISCUSSION

In this study, using SPIO-MRI technology in experimental liver studies, we have shown conclusively that rats and patients with NAFLD have impaired KC uptake function. The importance of these findings lies in the fact that hyper-endotoxaemia may be implicated in the pathogenesis of NAFLD since KCs through their uptake properties provide the predominant protective barrier against the egress of endotoxin from the portal to the systemic circulation.[27] Reduced KC uptake function may, therefore, lead to higher endotoxin levels in the systemic circulation, as has been observed in patients with NAFLD and in animal models of NASH.[7 25 28] Given that overproduction of, and increased sensitivity to, cytokines such as tumour necrosis factor α and interleukin 1β from KCs[10 28] is also implicated in the pathogenesis of NAFLD, failure of KCs to clear endotoxin because of defective uptake function may further drive the production of these proinflammatory cytokines by KCs.

The impairment of KC uptake function was not due to a decrease in the number of KCs because these were raised both in experimental NASH livers compared with controls, and in patients with NAFLD compared with CH-C controls. In addition, KC uptake function as assessed by SPIO-MRI, in healthy volunteers was not different from that of patients with CH-C, but was different from that of patients with NAFLD. The reduced KC uptake function in patients with NAFLD, however, worsened with the degree of hepatic steatosis but, intriguingly though, was not related to the NAS. The mechanisms underlying this unexpected finding form part of ongoing studies in our group. We also compared the RSE on SPIO-MRI between the NASH (NAS ≥5; n=13) and non-NASH groups (NAS ≤4; n=7), and between the NASH and simple steatosis groups (NAS <4). We found no differences between the NASH group (21.04±6.79%) and non-NASH group (18.73±4.01%, p=0.485), nor between the NASH group (21.04±6.79%) and the simple steatosis group (18.53±4.45%, p=0.486).

Our animal data support previous studies that have shown defective KC uptake function in models of NASH.[9] In addition, Moriyasu *et al*[29] using ultrasonography showed reduced KC uptake function in patients with NASH. However, while ultrasonographic evaluation of KC function may be influenced by altered hepatic microcirculation, the SPIO-MRI methods described here have controlled for possible microcirculatory changes.

A possible criticism of our study is that we did not directly measure endotoxin levels in our patients with NAFLD and thus the reduced uptake function may not be of pathophysiological significance. However, if it is accepted that endotoxin is of importance in NAFLD and that KCs, as argued above, provide the main defensive barrier to endotoxin, then in the presence of defective KC uptake function, endotoxin levels would be expected to rise, as has indeed been shown.[6 7] The mechanism underlying the observed reduction in human KC uptake function remains to be investigated but may be related to defective leptin signalling, as previously described in models of NASH[9 30 31] or it may be related to saturation of uptake mechanisms by, for example, KC engulfment of apoptotic bodies or erythrocytes, as has been previously observed in NASH.[32 33]

In conclusion, we have shown using an SPIO-MRI technique that KC uptake function is defective in experimental NAFLD and in patients with NAFLD. This defective uptake function may be responsible for the observed raised levels of endotoxin that have previously been implicated in the pathogenesis of NAFLD.

Acknowledgements We are indebted to the technicians in the Department of Radiology, Kochi Medical School Hospital, for invaluable technical assistance with the SPIO-MRI studies.

Funding Grants-in-Aid for Scientific Research (C) 2006 Grant # 17590656, The Ministry of Education, Science, Sports and Culture, Japan; Wellcome Trust, UK (JAO).

Competing interests None.

Patient consent Obtained.

Provenance and peer review Not commissioned; externally peer reviewed.

REFERENCES

1. **Ioannou GN,** Boyko EJ, Lee SP. The prevalence and predictors of elevated serum aminotransferase activity in the United States in 1999–2002. *Am J Gastroenterol* 2006;**101**:76–82.
2. **James O,** Day C. Non-alcoholic steatohepatitis: another disease of affluence. *Lancet* 1999;**353**:1634–6.
3. **Ekstedt M,** Franzen LE, Mathiesen UL, *et al*. Long-term follow-up of patients with NAFLD and elevated liver enzymes. *Hepatology* 2006;**44**:865–73.
4. **Creely SJ,** McTernan PG, Kusminski CM, *et al*. Lipopolysaccharide activates an innate immune system response in human adipose tissue in obesity and type 2 diabetes. *Am J Physiol Endocrinol Metab* 2007;**292**:E740–7.
5. **Velayudham A,** Dolganiuc A, Ellis M, *et al*. VSL#3 probiotic treatment attenuates fibrosis without changes in steatohepatitis in a diet-induced nonalcoholic steatohepatitis model in mice. *Hepatology* 2009;**49**:989–97.

6. **Thuy S,** Ladurner R, Volynets V, *et al*. Nonalcoholic fatty liver disease in humans is associated with increased plasma endotoxin and plasminogen activator inhibitor 1 concentrations and with fructose intake. *J Nutr* 2008;**138**:1452–5.
7. **Ruiz AG,** Casafont F, Crespo J, *et al*. Lipopolysaccharide-binding protein plasma levels and liver TNF-alpha gene expression in obese patients: evidence for the potential role of endotoxin in the pathogenesis of non-alcoholic steatohepatitis. *Obes Surg* 2007;**17**:1374–80.
8. **Gao Y,** Song LX, Jiang MN, *et al*. Effects of traditional chinese medicine on endotoxin and its receptors in rats with non-alcoholic steatohepatitis. *Inflammation* 2008;**31**:121–32.
9. **Loffreda S,** Yang SQ, Lin HZ, *et al*. Leptin regulates proinflammatory immune responses. *FASEB J* 1998;**12**:57–65.
10. **Diehl AM.** Nonalcoholic steatosis and steatohepatitis IV. Nonalcoholic fatty liver disease abnormalities in macrophage function and cytokines. *Am J Physiol Gastrointest Liver Physiol* 2002;**282**:G1–5.
11. **Tilg H,** Diehl AM. Cytokines in alcoholic and nonalcoholic steatohepatitis. *N Engl J Med* 2000;**343**:1467–76.
12. **Fox ES,** Broitman SA, Thomas P. Bacterial endotoxins and the liver. *Lab Invest* 1990;**63**:733–41.
13. **Imai Y,** Murakami T, Yoshida S. Superparamagnetic iron oxide-enhanced magnetic resonance images of hepatocellular carcinoma: correlation with histological grading. *Hepatology* 2000;**32**:205–12.
14. **Ward J,** Guthrie JA, Scott DJ, *et al*. Hepatocellular carcinoma in the cirrhotic liver: double-contrast MR imaging for diagnosis. *Radiology* 2000;**216**:154–62.
15. **Elizondo G,** Weissleder R, Stark DD, *et al*. Hepatic cirrhosis and hepatitis: MR imaging enhanced with superparamagnetic iron oxide. *Radiology* 1990;**174**:797–801.
16. **Kato N,** Ihara S, Tsujimoto T, *et al*. Effect of resovist on rats with different severities of liver cirrhosis. *Invest Radiol* 2002;**37**:292–8.
17. **Tanimoto A,** Oshio K, Suematsu M, *et al*. Relaxation effects of clustered particles. *J Magn Reson Imaging* 2001;**14**:72–7.
18. **Hirose A,** Ono M, Saibara T, *et al*. Angiotensin II type 1 receptor blocker inhibits fibrosis in rat nonalcoholic steatohepatitis. *Hepatology* 2007;**45**:1375–81.
19. **Koteish A,** Diehl AM. Animal models of steatosis. *Semin Liver Dis* 2001;**21**:89–104.
20. **Lawaczeck R,** Bauer H, Frenzel T, *et al*. Magnetic iron oxide particles coated with carboxydextran for parenteral administration and liver contrasting. Pre-clinical profile of SH U555A. *Acta Radiol* 1997;**38**:584–97.
21. **Asanuma T,** Hirano Y, Yamamoto K, *et al*. MR imaging of hepatic injury in the LEC rat under a high magnetic field (7.05 T). *J Vet Med Sci* 1999;**61**:239–44.
22. **Asanuma T,** Ohkura K, Yamamoto T, *et al*. Three-dimensional magnetic resonance imaging of lung and liver tumors in mice by use of transversal multislice magnetic resonance images. *Comp Med* 2001;**51**:138–44.
23. **Bhunchet E,** Eishi Y, Wake K. Contribution of immune response to the hepatic fibrosis induced by porcine serum. *Hepatology* 1996;**23**:811–7.
24. **Park SH,** Kim PN, Kim KW, *et al*. Macrovesicular hepatic steatosis in living liver donors: use of CT for quantitative and qualitative assessment. *Radiology* 2006;**239**:105–12.
25. **Kleiner DE,** Brunt EM, Van Natta M, *et al*. Design and validation of a histological scoring system for nonalcoholic fatty liver disease. *Hepatology* 2005;**41**:1313–21.
26. **Ijaz S,** Yang W, Winslet MC, *et al*. Impairment of hepatic microcirculation in fatty liver. *Microcirculation* 2003;**10**:447–56.
27. **Farrell GC.** Is bacterial ash the flash that ignites NASH? *Gut* 2001;**48**:148–9.
28. **Solga SF,** Diehl AM. Non-alcoholic fatty liver disease: lumen-liver interactions and possible role for probiotics. *J Hepatol* 2003;**38**:681–7.
29. **Moriyasu F,** Iijima H, Tsuchiya K, *et al*. Diagnosis of NASH using delayed parenchymal imaging of contrast ultrasound. *Hepatol Res* 2005;**33**:97–9.
30. **Li Z,** Lin H, Yang S, *et al*. Murine leptin deficiency alters Kupffer cell production of cytokines that regulate the innate immune system. *Gastroenterology* 2002;**123**:1304–10.
31. **Yang SQ,** Lin HZ, Lane MD, *et al*. Obesity increases sensitivity to endotoxin liver injury: implications for the pathogenesis of steatohepatitis. *Proc Natl Acad Sci U S A* 1997;**94**:2557–62.
32. **Canbay A,** Feldstein AE, Higuchi H, *et al*. Kupffer cell engulfment of apoptotic bodies stimulates death ligand and cytokine expression. *Hepatology* 2003;**38**:1188–98.
33. **Otogawa K,** Kinoshita K, Fujii H, *et al*. Erythrophagocytosis by liver macrophages (Kupffer cells) promotes oxidative stress, inflammation, and fibrosis in a rabbit model of steatohepatitis: implications for the pathogenesis of human nonalcoholic steatohepatitis. *Am J pathol* 2007;**170**:967–80.

Gut 2010;**59**:258–266. doi:10.1136/gut.2009.176651

Biochimica et Biophysica Acta 1801 (2010) 655–664

Contents lists available at ScienceDirect

Biochimica et Biophysica Acta

journal homepage: www.elsevier.com/locate/bbalip

Deletion of tumor necrosis factor-α receptor type 1 exacerbates insulin resistance and hepatic steatosis in aromatase knockout mice

Katsumi Toda [a,*], Yoshihiro Hayashi [b], Toshiji Saibara [c]

[a] Department of Biochemistry, Kochi University, School of Medicine, Nankoku, Kochi 783-8505, Japan
[b] Department of Pathology, Kochi University, School of Medicine, Nankoku, Kochi 783-8505, Japan
[c] Department of Gastroenterology and Hepatology, Kochi University, School of Medicine, Nankoku, Kochi 783-8505, Japan

ARTICLE INFO

Article history:
Received 17 August 2009
Received in revised form 15 February 2010
Accepted 4 March 2010
Available online 11 March 2010

Keywords:
Aromatase
Estrogen
Fatty acid
Hepatic steatosis
Insulin resistance
Tumor necrosis factor-α receptor type 1

ABSTRACT

The relevance of estrogen functions in lipid metabolism has been suggested in patients with estrogen-signaling deficiencies. Their importance was further implied by studies in estrogen-deficient mice (ArKO mice), which progressively developed hepatic steatosis. As circulating tumor necrosis factor (TNF)-α levels are known to positively correlate with disturbances in lipid metabolism, we investigated the impact of the loss of TNF-α signaling on carbohydrate and lipid metabolism in ArKO mice. Histological examinations of the livers of mice at 5 months of age revealed that ArKO male mice lacking the TNF-α receptor type 1 (TNFR1) gene (ArKO/TNFR1KO) or both the TNFR 1 and 2 genes (ArKO/TNFR1&2KO) developed more severe hepatic steatosis than ArKO or ArKO/TNFR2KO mice. Serum analyses demonstrated a clear increase in cholesterol and insulin levels in the ArKO/TNFR1KO mice compared with the ArKO mice. Glucose- and insulin-tolerance tests further revealed exacerbation of the systemic insulin resistant phenotype in the ArKO/TNFR1KO mice. Hepatic expression of lipogenic genes including fatty-acid synthase and stearoyl-Coenzyme A desaturase 1 were more markedly upregulated in the ArKO/TNFR1KO mice than the ArKO mice. These findings indicate that under estrogen-deficient physiological conditions, hepatic lipid metabolism would benefit from TNF-α mediated signaling via TNFR1.

1. Introduction

Several lines of evidence have indicated the involvement of a variety of inflammatory processes in the development of obesity and obesity-associated pathology [1,2]. Indeed, inflammatory pathways are upregulated in obese adipose tissue, leading to increased expression of downstream cytokines. It has been proposed that tumor necrosis factor (TNF)-α is a candidate mediator of obesity-related inflammation. This is based on the following observations: 1) TNF-α is overexpressed in the adipose tissues of obese rodent models; 2) targeted deletion of the gene(s) for TNF-α or its two receptors, p55 TNF-α receptor 1 (TNFR1) and p75 TNF-α receptor 2 (TNFR2), significantly improves systemic insulin sensitivity in diet-induced obesity; 3) chronic exposure to TNF-α induces insulin resistance both in vitro and in vivo; 4) treatment with neutralizing soluble TNF receptors improves insulin sensitivity in obese rodent models [3–7]. Consistent with these animal studies, clinical studies revealed that TNF-α expression was markedly increased in adipose tissue and skeletal muscle in insulin resistant patients and that a restoration of insulin sensitivity was associated with a substantial decrease in serum TNF-α levels in obese patients [8,9].

The involvement of estrogens in the regulation of carbohydrate and lipid metabolism was robustly demonstrated by studies in genetically engineered mice including aromatase gene (*Cyp19*)-knockout (ArKO) mice [10–13]. *Cyp19* belongs to the cytochrome P450 superfamily and encodes an enzyme catalyzing the conversion of androgens to estrogens in various mammalian tissue-sites [14]. Our previous study demonstrated that disruption of *Cyp19* caused deregulation of lipid and glucose metabolism, resulting in the development of obesity, insulin resistance, and hepatic steatosis in a sexually dimorphic manner [10,15]. Furthermore, supplementation with 17β-estradiol (E2) restored the regulatory activities of the metabolism, resulting in recovery of the metabolic parameters to the levels of the wild-type (WT) mice [10,11,15]. These observations, therefore, support the fundamental role of estrogens in metabolic regulation.

We hypothesized that abolishing the signaling and function of TNF-α might improve the serum and hepatic phenotypes of ArKO mice. To test this hypothesis, ArKO mice lacking the gene(s) for TNFR1, TNFR2, or both were generated. We report here that the serum and hepatic phenotypes caused by inactivation of the aromatase gene

Abbreviations: ArKO, aromatase knockout; $ArKO_M$, aromatase knockout with minimal steatosis; $ArKO_{FL}$, aromatase knockout with hepatic steatosis; Cyp, cytochrome P450; ERα, estrogen receptor α; GTT, glucose tolerance test; ITT, insulin-tolerance test; TNF-α, tumor necrosis factor-α; TNFR1, TNF-α receptor 1; WT, wild-type

* Corresponding author. Tel./fax: +81 88 880 2316.
E-mail address: todak@kochi-u.ac.jp (K. Toda).

1388-1981/$ – see front matter © 2010 Elsevier B.V. All rights reserved.
doi:10.1016/j.bbalip.2010.03.002

were not ameliorated but rather exacerbated by the deletion of the TNF-α signaling pathway through TNFR1. These data demonstrate that the TNF-α mediated pathway is beneficial for glucose and fatty-acid metabolism under physiological conditions when estrogen functions are limited.

2. Materials and methods

2.1. Experimental animals

The animal experiments were carried out according to the guidelines of our Institutional Animal Regulations. All animals were maintained under a 12 h-light/dark cycle at 22–25 °C and given water and phytoestrogen-low rodent chow (NIH-07PLD, Oriental Yeast Ltd., Tokyo, Japan) ad libitum. *Cyp19* was disrupted by homologous recombination [16], and the genetic background was unified to C57BL/6j by repeated backcrossing [17]. Because of the infertility caused by inactivation of *Cyp19*, ArKO mice were generated by intercrossing with *Cyp19* heterozygous mice ($Ar^{+/-}$). TNFR double knockout (TNFR1&2KO) mice (B6;129STTnfrsf1a^{tm1Imx}Tnfrsf1b^{tm1Imx}) [18] were purchased from the Jackson Laboratory. By repeated crossing of TNFR1&2KO mice with $Ar^{+/-}$ mice, $Ar^{+/-}$/TNFR1KO, $Ar^{+/-}$/TNFR2KO, and $Ar^{+/-}$/TNFR1&2KO mice were generated. Then, ArKO/TNFR1KO, ArKO/TNFR2KO, and ArKO/TNFR1&2KO mice were obtained by intercrossing of $Ar^{+/-}$ mice with each TNFR genotype. Male mice at 2 or 5 months of age were used for this study. Their body weights were determined every 2 weeks beginning at 6 weeks of age. Their food-intake per day was measured using mice at 2 or 5 months of age.

2.2. Histological examination

Livers were removed from the mice at 2, 3, 4, or 5 months of age, fixed in a solution of 10% (v/v) buffered formalin for 24 h, dehydrated in graded ethanol, and then embedded in paraffin. The samples were cut into 3 μm-thick sections and stained with hematoxylin–eosin. The development of hepatic steatosis was evaluated qualitatively by microscopy based on the presence of liver cells filled with numerous lipid droplets.

2.3. Measurement of glucose, cholesterol, triglycerides, free fatty acids, leptin, insulin, adiponectin, and TNF-α

Tail blood was collected via vein nicks of fed mice for measurement of leptin and TNF-α, or of mice fasted for 16 h overnight with full access to water for measurement of glucose, cholesterol, triglycerides, free fatty acids, insulin and adiponectin. The concentrations of serum cholesterol, serum triglycerides, and plasma free fatty acids were measured by colorimetric methods using the Triglyceride E-Test, Cholesterol T-Test, and NEFA C-Test, respectively (Wako Pure Chemical Industries Ltd., Osaka, Japan). Serum leptin, serum insulin, plasma adiponectin, and plasma TNF-α were determined by using enzyme-linked immunoassay kits (BioVendor Laboratorni medicina a.s., Modrice Czech Republic, Mercodia AB, Uppsala, Sweden, R&D Systems, Inc., MN55413, USA, and Thermo Scientific, Rockford, IL61105, USA, respectively). Blood glucose concentration was measured with Glutest Ace and Glutest Sensor (Sanwa Kagaku Kenkyusho Co., Nagoya, Japan) before glucose challenge or at 30, 60, and 120 min after the intraperitoneal injection (ip) of glucose (2 mg glucose/g of body weight in saline) (glucose tolerance test, GTT) [15]. Insulin sensitivity was assessed using an insulin-tolerance test (ITT) as described previously [15]. The fed mice were given an ip injection of insulin from the bovine pancreas at a dose of 0.75 mU/g of body weight (Sigma-Aldrich, Inc., St. Louis, MO63103, USA, Cat. No. I1882), and blood glucose concentrations were measured at 0, 10, 30, 60, and 120 min after injection of insulin.

2.4. Secretion of TNF-α in response to lipopolysaccharide treatment

Mice at 5 months of age with mean body weights of 33.8 ± 0.7 g and 37.9 ± 0.8 g for WT and ArKO mice, respectively ($n = 5$ for each genotype) were injected ip with saline or lipopolysaccharide (LPS) (*Escherichia coli* 0127 B8, Sigma-Aldrich, Inc., St. Louis, MO) at a dose of 10 ng/g of body weight. After 60 min, 0.1 ml blood was collected from the tail vein using a tube containing 10 μl of 0.25 M EDTA, and plasma were prepared and stored at −20 °C until use. Basal plasma levels of TNF-α were also measured using untreated mice ($n = 7$) at 2, 3, 4 and 5 months of age.

2.5. Analysis of mRNA expression

Messenger RNA analysis was performed by Northern blotting or by quantitative real-time PCR (QRT-PCR) for carbohydrate responsive element-binding protein (ChREBP) and sterol regulatory element-binding protein-1 (SREBP-1). Three mice for each strain were sacrificed at 2 and 5 months of age. Liver was dissected, frozen on liquid nitrogen, and stored at −80 °C until use. Total RNA was prepared from individual liver samples by the method of Zarlenga and Gamble [19]. Equal amounts of the total RNA from the same strain were pooled. Fifteen micrograms of the pooled RNA were separated on a 0.8% agarose gel and transferred to a nylon membrane. The membranes were incubated with ^{32}P-labeled cDNA probes and analyzed on a Fuji system analyzer (Fuji Photo Film, Tokyo, Japan) for quantification of band intensity. The probes (gene symbol, accession number) used for Northern blotting were acetyl-CoA carboxylase 1 (Acaca, NM_133360); acyl-Coenzyme A dehydrogenase, medium chain (Acadm, NM_007382); acyl-Coenzyme A oxidase 1 (Acox1, NM_015729); carnitine palmitoyltransferase 1a, liver (Cpt1a, NM_013495); catalase (Cat, L25069); cytochrome P450, family 2, subfamily e, polypeptide 1 (Cyp2e1, NM_021282); cytochrome P450, family 7, subfamily a, polypeptide 1 (Cyp7a1, NM_007824); fatty acid synthetase (Fasn, NM_007988); glutathione peroxidase 1 (Gpx1, NM_008160); malic enzyme 1, NADP(+)-dependent, cytosolic (Me1, NM_008615.2); microsomal triglyceride transfer protein (Mttp, NM_008642); stearoyl-Coenzyme A desaturase 1 (Scd1, NM_009127); and glyceraldehyde-3-phosphate dehydrogenase (Gapdh, NM_008084). Quantitative changes in mRNA levels for three independent experiments were calculated by a BAS 2000 III (Fiji film Inc., Tokyo Japan) to show their ratio to the levels in the wild-type (WT) mice group.

Total RNA (1 μg) was reverse-transcribed for 1 h at 37 °C in a 25-μl final volume reaction using 200 U of M-MLV reverse transcriptase (Invitrogen Corporation, Carlsbad, CA92008, USA) according to the manufacturer's instructions. To quantify the mRNA expression levels of ChREBP and SREBP-1, QRT-PCR analysis was performed starting with 16 ng of reverse-transcribed total RNA in a final volume of 12.5-μl using SYBR® *Premix Ex* Taq™II in a light cycler instrument (Takara Bio inc., Shiga JAPAN). Primers used for ChREBP (NM_021455) were (sense) 5′-CTGGGGACCTAAACAGGAGC-3′, (antisense) 5′-GAAGCCACCCTA-TAGCTCCC-3′ (amplified size, 166 bp); for SREBP-1 (NM_011480) were (sense) 5′-ACCGTCACTTCCAGCTAGAC-3′, (antisense) 5′-CCAC-TAAGGTGCCTACAGAGC-3′ (181 bp); and for cyclophilin A (NM_008907) were (sense) 5′-ATGGCACTGGCGGCAGGTCC-3′, (anti-sense) 5′-TTGCCATTCCTGGACCCAAA-3′ (241 bp). The PCR conditions were as described [20]. The relative quantification for a given gene was corrected to the cyclophilin mRNA values.

2.6. Preparation of nuclear extracts and immunoblot analysis of ChREBP and SREBP expression

Hepatic nuclear extracts were prepared from mice at 2 and 5 months of age using NE-PER® Nuclear and Cytoplasmic Extraction Reagents (Thermo Scientific, Rockford, IL61105, USA) according to the

Table 1
Ablation of TNFR1 accelerates fatty liver development.

Tnfr loci / Cyp19 locus	WT	TNFR1 KO	TNFR2 KO	TNFR1&2 KO
WT	0/6 (0%)	1/20 (5%)	0/7 (0%)	1/6 (17%)
ArKO	16/32 (50%)	43/48* (89%)	4/12 (33%)	11/13** (85%)

The accumulation of fat in the livers of TNFR1KO and ArKO/TNFR1KO mice was examined microscopically at various ages. The numerals over and under the bar, respectively, indicate the number of mice showing severe hepatic steatosis and the number of mice examined. The numerals in parentheses indicate the percentage of mice showing hepatic steatosis. Hepatic steatosis became evident after 4 months of age in the ArKO/TNFR1KO mice. ND indicates not determined. * $p<0.0001$, ** $p<0.02$.

manufacturer's instructions. Protein concentration was determined using BCA Protein Assay™ reagents (PIERCE, Rockford, IL61105, USA) using bovine serum albumin as a standard. Proteins (50 μg) were subjected to SDS-PAGE analysis on a 10% gel and electrotransferred onto polyvinylidene difluoride membranes (Milipore Corporation, Billerica, MA 01821, USA). Rabbit anti-SREBP-1 and anti-ChREBP polyclonal antibodies (sc-366; dilution 1:2000 and sc-33764; dilution 1:1000, respectively, Santa Cruz Biotechnology, Santa Cruz, CA95060, USA) as the primary antibody were incubated with the membranes for 12 h at 4 °C. Rabbit polyclonal anti-histone H3 antibody (H0164; dilution 1:10,000, Sigma-Aldrich, Saint Louis, MO63103, USA) was used as a loading control. The membranes were then incubated with anti-rabbit horseradish peroxidase-conjugated IgG (#7074; dilution 1:2000, Cell Signaling Technology, Danvers, MA01923, USA) as the second antibody for 1 h at 25 °C, followed by incubation with Immobilon™Western reagents (Milipore Corporation). Visualization and quantification of signals were performed using LAS-4000mini (FUJIFILM Corporation, Tokyo, Japan). The antibodies for ChREBP and SREBP-1 detected bands at 95 kDa and 70 kDa, respectively, and the relative quantification for given signals was corrected to the histone H3 values.

2.7. Statistical analysis

Data are expressed as the mean ± SEM, and analyzed using Students *t*-test, Mann–Whitney's *U* test, two-way ANOVA, and Chi-square test when they were applicable. *P* values less than 0.05 were considered significant.

3. Results

3.1. Hepatic histology

As described previously [10,15], ArKO male mice fed a diet of phytoestrogen-low chow gradually accumulated abdominal fat and developed hepatic steatosis, although there was a slight variation in the phenotype at 5 months of age; approximately 50% of ArKO mice developed hepatic steatosis (Table 1). In contrast, more than 80% of the ArKO/TNFR1KO and ArKO/TNFR1&2KO mice displayed marked microvesicular steatosis at 5 months of age (Table 1 and Fig. 1). Hepatic steatosis became evident at 4 months of age in the ArKO/TNFR1KO mice (Table 2). In contrast, deletion of TNFR2 did not exert a detrimental effect on the hepatic phenotype at 5 months of age, compared with the ArKO mice. Their wild-type (WT) siblings did not develop hepatic steatosis at this age (Table 1). Because minimum hepatic effect was observed in the ArKO/TNFR2 mice, following analyses were performed with ArKO, ArKO/TNFR1KO, TNFR1KO and WT mice.

3.2. Measurement of metabolic parameters

The mean body weights of the WT, ArKO, TNFR1KO, and ArKO/TNFR1KO mice were similar until 4 months of age. The weights of the ArKO, TNFR1KO, and ArKO/TNFR1KO mice at 5 months of age were also similar to each other, but were heavier than that of the WT mice (WT; 33.1 ± 2.0 g ($n=8$) vs. ArKO 40.4 ± 1.3 g ($n=23$) ($p<0.03$), vs. TNFR1KO; 38.5 g ± 1.5 g ($n=7$) ($p<0.06$), vs. ArKO/TNFR1KO; 40.3 ± 0.9 g ($n=6$) ($p<0.004$)) (Fig. 2). Both the TNFR1KO and ArKO/

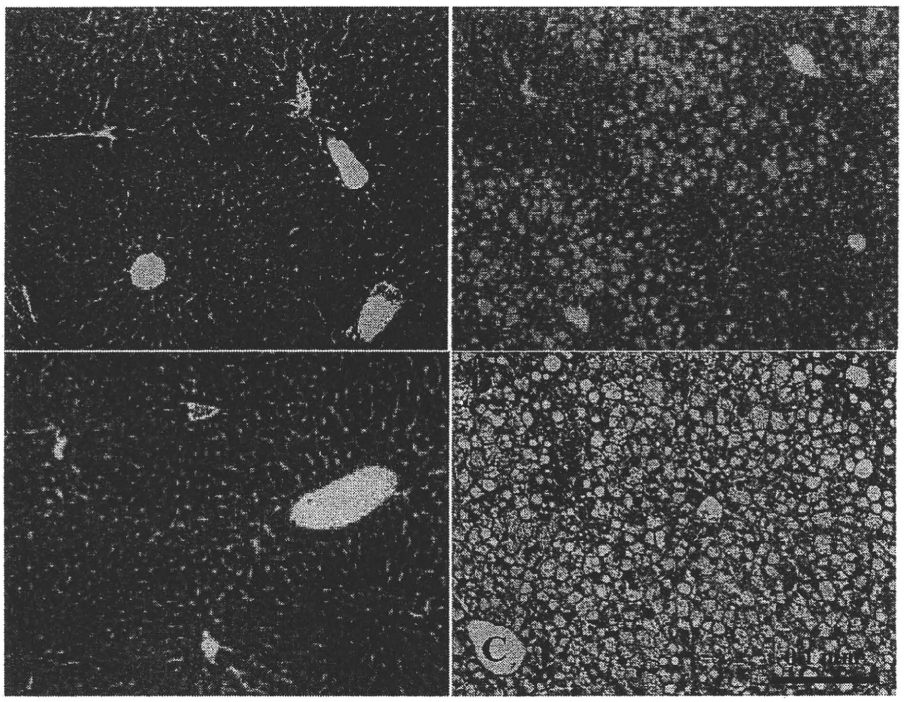

Fig. 1. Hepatic histology in ArKO, TNFR1KO, and ArKO/TNFR1KO mice. Hematoxylin and eosin staining of liver sections from fed ArKO/TNFR1KO mice at 2 months of age (A) and ArKO (B), TNFR1KO (C), and ArKO/TNFR1KO (D) mice at 5 months of age. Note that increased hepatic steatosis was evident in ArKO/TNFR1KO mice at 5 months of age, which displayed an accumulation of microvesicular lipid droplets in the regions around the central veins (c). Scale bar: 100 μm.

Table 2
Age-dependent development of fatty liver.

Age	2M	3M	4M	5M
TNFR1 KO	0/4 (0%)	ND	ND	1/20 (5%)
ArKO/TNFR1 KO	1/9 (11%)	1/9 (11%)	4/5 (80%)	43/48* (89%)

The accumulation of fat in the livers of TNFR1KO and ArKO/TNFR1KO mice was examined mic ages. The numerals over and under the bar, respectively, indicate the number of mice showing seve the number of mice examined. The numerals in parentheses indicate the percentage of mice sho Hepatic steatoşis became evident after 4 months of age in the ArKO/TNFR1KO mice. ND indicates *$p<0.0001$, **$p<0.02$.

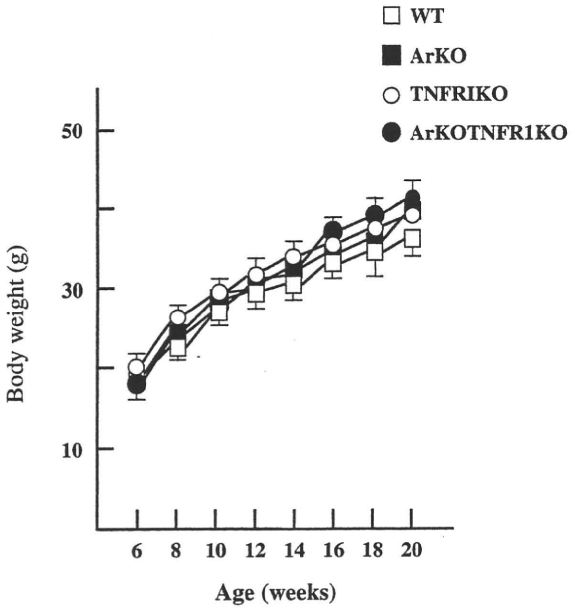

Fig. 2. Measurement of body weight. Body weights were measured every 2 weeks beginning at 6 weeks of age.

TNFR1KO mice showed increased food-intake at 2 months of age ($p<0.05$, vs. WT mice, and $p<0.001$, ArKO/TNFR1KO mice vs. ArKO mice). However, only the TNFR1KO mice exhibited a food-intake increase at 5 months of age ($p<0.05$, vs. WT mice) (Fig. 3A). Blood glucose levels were similar among the fasted animal groups at 2 months of age; whereas the fasting serum insulin levels in the TNFR1KO and ArKO/ TNFR1KO mice were significantly reduced compared to those in the WT and ArKO mice at 2 months of age ($p<0.05$ and $p<0.01$, vs. WT mice, respectively) (Fig. 3B and C). At 5 months of age, fasting blood glucose levels were significantly elevated in the ArKO and ArKO/TNFR1KO mice compared to the other two groups ($p<0.05$ and $p<0.01$, respectively) (Fig. 3B). However no significant difference was observed between ArKO and ArKO/TNFR1KO mice. There was no significant difference in fasting insulin levels between the WT and ArKO mice, although moderate pancreatic beta cell dysfunction was suggested in the ArKO mice [21]. Contrarily, the fasting serum insulin levels in the ArKO/TNFR1KO mice were four times higher than those in the WT and ArKO mice ($p<0.001$, vs. WT mice, and $p<0.001$ vs. ArKO mice, respectively) (Fig. 3C), suggesting the development of severe insulin resistance. No significant differences were observed in the circulating levels of triglycerides, free fatty acids, or cholesterol among these four groups at 2 months of age (Fig. 3D–F). The ArKO/TNFR1KO mice showed a significant elevation in serum cholesterol levels at 5 months of age compared to the other groups ($p<0.001$, vs. WT mice, and $p<0.01$, vs. ArKO mice) (Fig. 3F).

Since TNFRKO and WT mice showed significant differences in food-intake, we measured serum leptin and plasma adiponectin levels. TNFR1KO, but not ArKO/TNFR1KO mice showed significantly lower serum leptin levels as compared to the other groups at 2 months of age (Fig. 3G). Serum leptin levels significantly increased in ArKO and ArKO/TNFR1KO mice at 5 months of age ($p<0.05$, vs. WT mice, and $p<0.05$, ArKO/TNFR1KO mice vs. ArKO mice), indicating that less apparent correlation was detected between food-intake and mouse genotypes at 5 months of age. In addition, we detected no significant differences in plasma adiponectin levels among the animal groups at 2 or 5 months of age (Fig. 3H).

3.3. GTT and ITT

To investigate the effects of deletion of TNF-α signaling on glucose homeostasis in estrogen-deficient male mice, glucose tolerance tests (GTT) and insulin-tolerance tests (ITT) were performed (Fig. 4). The GTT revealed that the ArKO mice displayed reduced blood glucose elimination compared to the WT mice, as reported previously [15]. A more prominent reduction in glucose-eliminating activity was observed in the ArKO/TNFR1KO mice ($p<0.001$, ArKO/TNFR1KO vs. mice with other genotypes). Furthermore, the ArKO/TNFR1KO mice revealed severely impaired insulin sensitivity compared to the WT and ArKO mice ($p<0.05$, ArKO/TNFR1KO vs. mice with other genotypes).

3.4. Expression of genes related to lipid metabolism in the liver

Alterations in the expression levels of a subset of genes related to lipid metabolism were examined next in the livers of the mice at 2 and 5 months of age, in order to detect the early transcriptional changes that precede the pathological manifestations of hepatic steatosis.

Enhanced mRNA expression of lipogenic and fatty-acid-oxidative genes was a characteristic feature of the estrogen-deficient mice at 2 months of age (Fig. 4A). The mRNA levels coding for the lipogenic enzymes, including Acaca, Me1, Fasn, and Scd1 were upregulated in the ArKO mice regardless of loss of the TNFR1 gene at 2 months of age compared to the levels in WT mice (1.6-fold, 1.3-fold, 5.3-fold, and 3.1-fold in the ArKO mice and 1.4-fold, 1.6-fold, 6.6-fold, and 4.6-fold in the ArKO/TNFR1KO mice, respectively) (Fig. 4C). In addition, the mRNA expression of genes encoding enzymes involving fatty-acid-oxidative reactions such as Cpt1a, Acox1, and Cat was also upregulated in the ArKO and ArKO/TNFR1KO livers (1.6-fold, 2.9-fold, and 3.1-fold in the ArKO mice and 1.4-fold, 2.2-fold, and 2.4-fold in the ArKO/TNFR1KO mice, respectively) (Fig. 4C). These results indicate that both lipogenic and fatty-acid-oxidative activities are enhanced under estrogen-deficient conditions at 2 months of age. Furthermore, the mRNA of Cyp7a1, which is a key enzyme for the clearance of cholesterol, was expressed 3.5 times more abundantly in the ArKO/TNFR1KO mice at 2 months of age.

As 50% of the ArKO mice developed severe hepatic steatosis at 5 months of age (Table 1), the ArKO mice at this age were divided into two groups for analysis of hepatic mRNA expression: one group of mice with hepatic steatosis ($ArKO_{FL}$) and the other with minimal steatosis ($ArKO_M$). The $ArKO_M$ mice revealed enhanced mRNA expression of lipogenic and fatty-acid-oxidative genes as observed in the ArKO mice at 2 months of age. In the $ArKO_{FL}$ mice, the mRNA expression of Acaca and Fasn were 0.7 and 0.5 times downregulated,

Fig. 3. Measurement of metabolic parameters. Various metabolic parameters were measured in blood samples from WT (open bar), ArKO (slashed bar), TNFR1KO (dotted bar), and ArKO/TNFR1KO (closed bar) mice at 2 and 5 months of age. (A) Food-intake (g/day), (B) fasting blood glucose ($n=11$–25), (C) fasting serum insulin ($n=5$–8), (D) fasting serum triglycerides ($n=10$), (E) fasting plasma free fatty acids ($n=10$), (F) fasting serum total cholesterol ($n=10$), (G) serum leptin ($n=7$) and (H) fasting plasma adiponectin ($n=5$–8) concentrations were measured. (a, and b, $p<0.05$ vs. WT mice, and $p<0.05$ vs. ArKO mice, respectively).

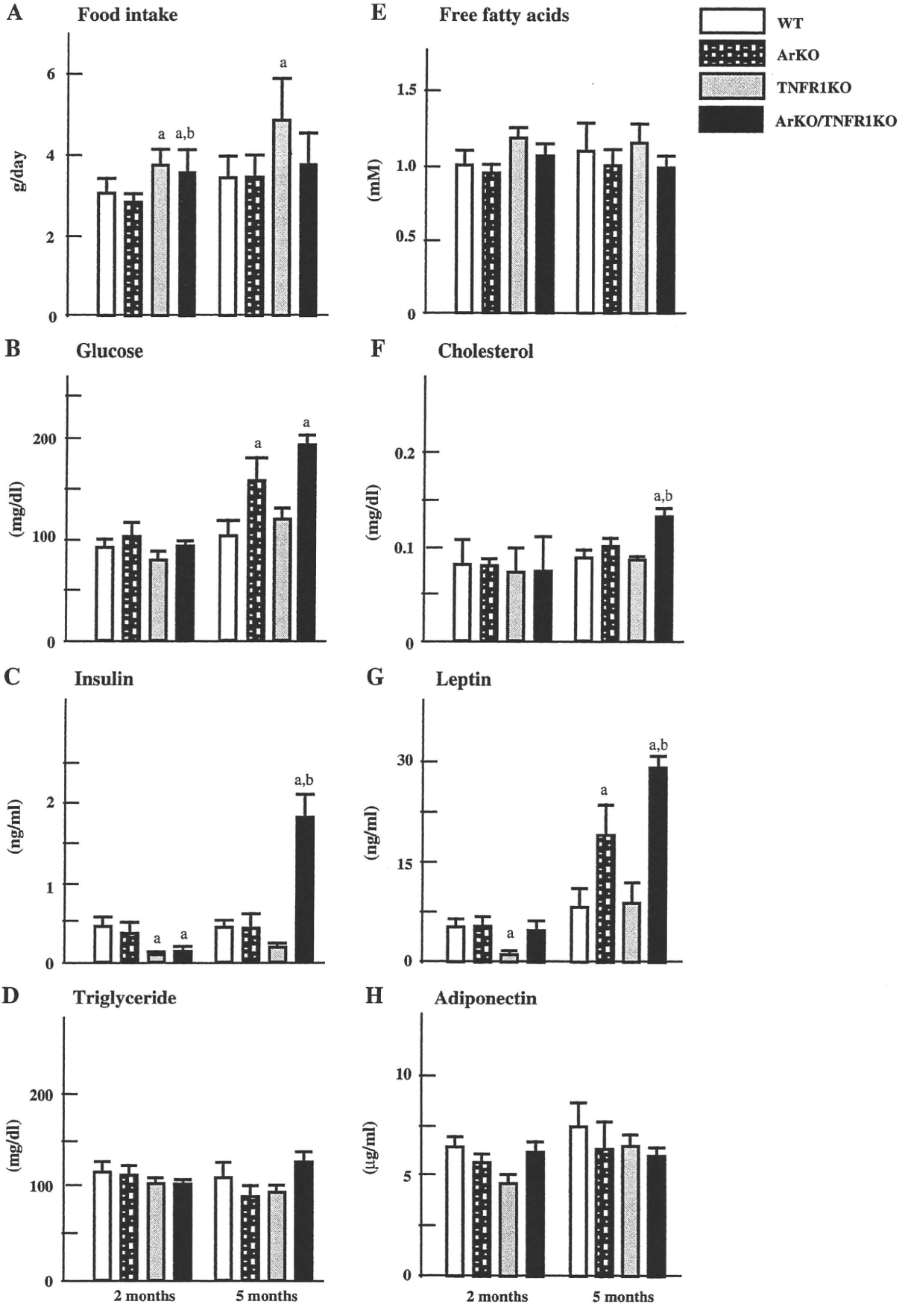
A
Food intake
g/day
6
4
2
0
a
a,b
a
B
Glucose
(mg/dl)
200
100
0
a
a
C
Insulin
(ng/ml)
2
1
0
a
a
a,b
D
Triglyceride
(mg/dl)
200
100
0
2 months
5 months
E
Free fatty acids
(mM)
1.5
1.0
0.5
0
F
Cholesterol
(mg/dl)
0.2
0.1
0
a,b
G
Leptin
(ng/ml)
30
15
0
a
a
a,b
H
Adiponectin
(μg/ml)
10
5
0
2 months
5 months
WT
ArKO
TNFR1KO
ArKO/TNFR1KO

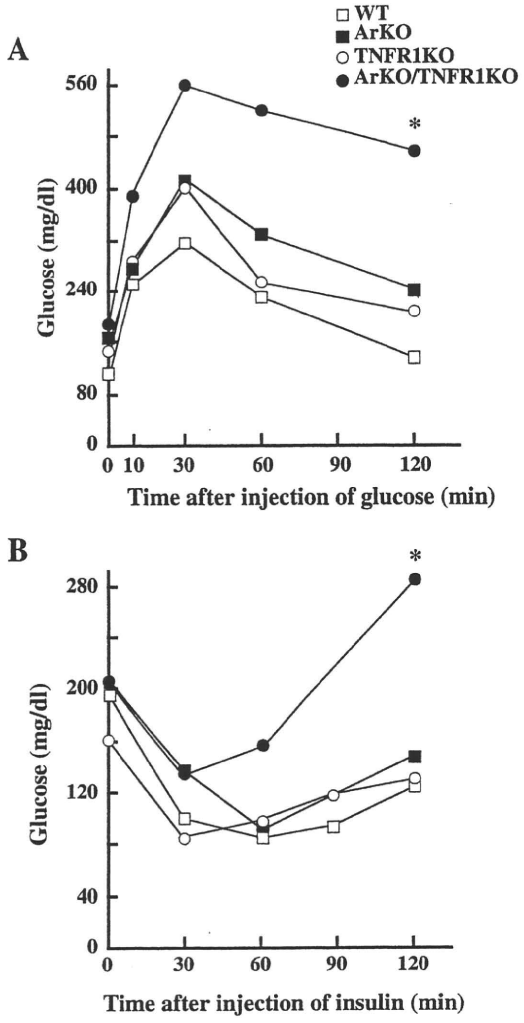

Fig. 4. ArKO/TNFR1KO mice display glucose intolerant and insulin resistant phenotypes. (A) Glucose tolerance tests were performed on WT (open squares), ArKO (closed squares), TNFR1KO (open circles), and ArKO/TNFR1KO (closed circles) mice that had been fasted for 16 h at 5 months of age. The animals were injected (ip) with 2 mg/g body weight of glucose. Blood glucose was measured before injection and 15, 30, 60, and 120 min after the injection. The results are expressed as mean blood glucose concentration ± SEM from five animals per genotype. (B) Insulin-tolerance tests were performed in fed WT, ArKO, TNFR1KO, and ArKO/TNFR1KO mice at 5 months of age. The mice were injected (ip) with 0.75 U/kg body weight of human recombinant insulin. Blood glucose was measured before injection and 30, 60, 90, and 120 min after the injection. The results are expressed as mean blood glucose concentration ± SEM. The asterisks indicate $p<0.001$, ArKO/TNFR1KO mice vs. WT mice).

respectively, and those of Me1 and Scd1 were 1.5 times upregulated compared to those in the $ArKO_M$ mice. Furthermore, the mRNA levels of genes related to fatty-acid oxidation in the $ArKO_{FL}$ mice were less abundant compared to those in the $ArKO_M$ mice except for Acadm (Fig. 4B), indicating that fatty-acid-oxidative activity was attenuated when hepatic steatosis developed in the ArKO mice, as reported previously [10]. In the ArKO/TNFR1KO mice, the expression levels of the lipogenic genes except for Acaca were sustained at high levels at 5 months of age, even after the development of severe hepatic steatosis. The expression of Gpx1 mRNA was not altered among the experimental animal groups (Fig. 5).

3.5. QRT-PCR and immunoblot analysis on expression of ChREBP and SREBP-1

Expression levels of mRNA for ChREBP and SREBP-1 and their nuclear protein contents in the livers were measured to study molecular mechanisms involved in the upregulation of lipogenic gene expression in the estrogen-deficient mice (Fig. 6). The ArKO and ArKO/TNFR1KO mice contained approximately double amounts of mRNA for the factors as compared to those of WT mice at 2 month of age ($p<0.05$, vs. WT mice, not significant between ArKO and ArKO/TNFR1KO mice). The mRNA levels for ChREBP and SREBP-1 in TNFR1KO mice were, respectively, 40% ($p<0.05$, vs. WT mice) and 70% of the WT mice levels at this age. Nuclear content of ChREBP in TNFR1KO mice, however, was 3-fold more than the other groups at 2 months of age ($p<0.05$, vs. WT mice). The nuclear contents of SREBP-1 did not show significant differences among the groups at 2 months of age.

At 5 months of age, TNFR1KO and ArKO/TNFR1KO mice, respectively, expressed twice more the amounts of mRNAs for ChREBP and SREBP-1 when compared to levels of the WT mice but without statistical significance. An increase in nuclear protein content of ChREBP was detected in ArKO mice displaying severe hepatic steatosis and TNFR1KO mice but not ArKO/TNFR1KO mice, which showed a significant decrease as compared to that of ArKO mice ($p<0.05$, vs. ArKO mice). Nuclear amounts of SREBP-1 were increased 2- to 3-fold in ArKO with severe steatosis, TNFR1KO ($p<0.005$, vs. WT mice) and ArKO/TNFR1KO mice over the WT levels. The summary of the expression analyses on ChREBP and SREBP-1 at 2 and 5 months of age was presented in Fig. 6C.

3.6. Secretion of TNF-α in ArKO mice

Estrogen-deficiency in ArKO mice might be a reason for the changes seen in their TNF-α levels, which worsened hepatic lipid metabolism. To examine this possibility, the basal plasma TNF-α levels and the levels secreted in response to LPS were determined using WT and ArKO mice showing relatively non-obese phenotypes at 5 months of age. We obtained no evidence showing significant differences in the basal plasma TNF-α levels between WT and ArKO mice at any ages examined (Fig. 7 and data not shown). Furthermore no significant differences were detected in the response to LPS-induced TNF-α levels (Fig. 7). These results indicate that estrogen-deficiency does not alter the systemic levels of TNF-α.

4. Discussion

TNF-α is a proinflammatory cytokine that plays a major role in the pathogenesis of autoimmune diseases and inflammatory disorders [22] and is also known to modulate insulin signaling in the liver either at sites downstream from the insulin receptor or through hepatic overproduction of very low density lipoproteins [23,24]. Elevation of TNF-α expression is thus thought to be associated with systemic insulin resistance [4]. However, TNF-α signaling has been demonstrated to be required for normal glucose homeostasis using db/db male mice, in which the loss of both TNFR1 and 2 genes causes severe hyperinsulinemia [25]. Thus, we wondered whether ArKO mice, which are predisposed to develop hepatic steatosis [10], would be protected from impairment of lipid metabolism by the blocking of TNF-α function.

As described previously [15], ArKO mice displayed hyperglycemia at 5 months of age. Nevertheless, GTT and ITT revealed less marked impairment in blood glucose elimination of ArKO mice when compared to the previous study [15]. Alternations in genetic background of ArKO mice, possibly owing to repeated backcrossing with C57BL/6j mice [17], might explain the phenotypic differences between the studies. The possible genetic alternations also link with the development of varying degrees of hepatic steatosis in the current ArKO mice. Nevertheless further studies are required to establish the reasons.

The hyperglycemia observed in the ArKO mice at 5 months of age might induce pancreatic β-cell dysfunction as reported recently, where E2 was demonstrated to protect insulin secretion through

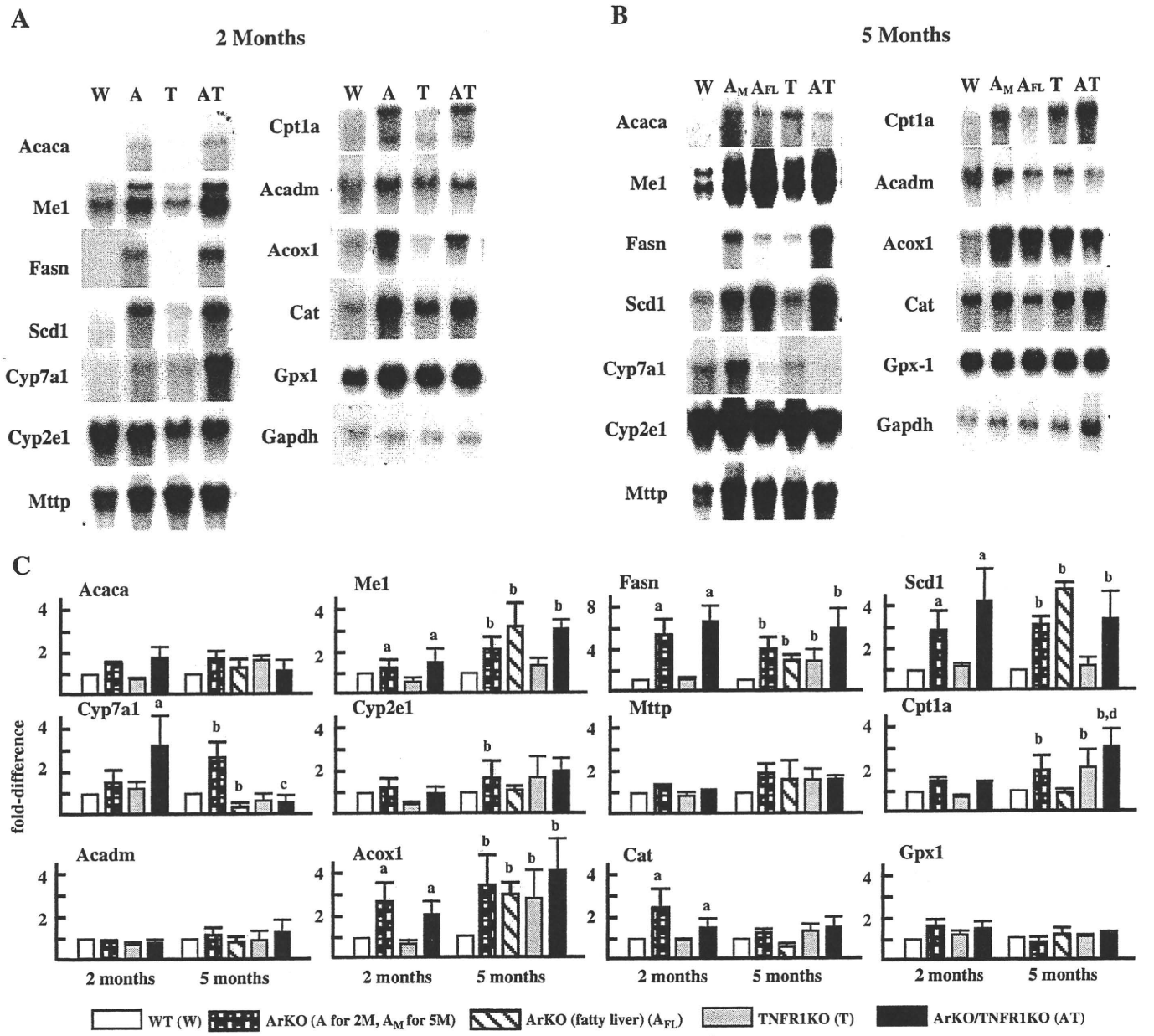

Fig. 5. Northern blot analysis. Total RNA extracted from the liver of WT (W), ArKO (A_M, A_{FL}), TNFR1KO (T), and ArKO/TNFR1KO (AT) mice at 2 (A) or 5 (B) months of age. RNA blotted onto nylon membranes were probed with ^{32}P-labeled cDNA probes as shown. GADPH was selected as a loading control. A_M and A_{FL} indicate ArKO mice that developed minimal and severe hepatic steatosis, respectively. (C) The bar-graphs illustrate fold-difference compared to the expression level in the livers of the WT mice. The bar-graphs illustrate fold-difference compared to the expression level in the livers of the WT mice. (a, b, c and d, $p<0.05$ vs. WT mice at 2 months, vs. WT mice at 5 months of age, vs. A_M mice at 5 months The expression of adiponectin is of age, and vs. A_{FL} mice at 5 months of age, respectively).

estrogen receptor (ER) α actions [21]; nevertheless, no statistically significant difference was detected in the serum insulin levels between the WT and ArKO mice. ArKO/TNFR1KO mice at this age displayed hyperinsulinemia in addition to their exacerbated glucose tolerant activity; the latter phenotype is a characteristic feature of estrogen-deficient mice and seems to be worsened by deletion of the TNFR1 gene possibly due to elevated action of gluconeogenesis. These observations indicate that the pancreatic β-cell dysregulation caused by E2 deficiency might involve a TNF-α mediated pathway that acts via TNFR1. As the ArKO/TNFR1KO mice also developed severe hepatic steatosis at this age, increased adiposity might cause hepatic metabolic abnormality and hyperinsulinemia; nevertheless, a causal relationship between hepatic lipid accumulation and systemic insulin resistance still remains debatable [26,27].

The decrease in the expression level of Fasn mRNA was marked in the ArKO mice with severe hepatic steatosis in addition to decreases in the mRNA of Cpt1a, Cat, and Cyp7a1, which is consistent with the previous observations in aged ArKO mice with hepatic steatosis [10]. By contrast, the ArKO/TNFR1KO mice, which also developed severe hepatic steatosis, maintained high levels of lipogenic gene expression including of Me1, Fasn, and Scd1. These observations suggest that TNF-α signaling through TNFR1 is required for the adaptation of hepatic cells to excessive fat accumulation via a reduction in fatty-acid synthesis. A marked elevation of Scd1 mRNA expression was notable even at the stage preceding the development of hepatic steatosis in the ArKO and ArKO/TNFR1KO mice. It has been reported that one product of Scd1, oleic acid, caused endoplasmic reticulum stress in the liver and worsened the pathology of hepatic steatosis [28]. Thus, unsaturated fatty acids, specifically monounsaturated fatty acids, synthesized in an uncontrolled fashion might be the primary event leading to metabolic abnormality in the livers of ArKO mice in the later stage of their life.

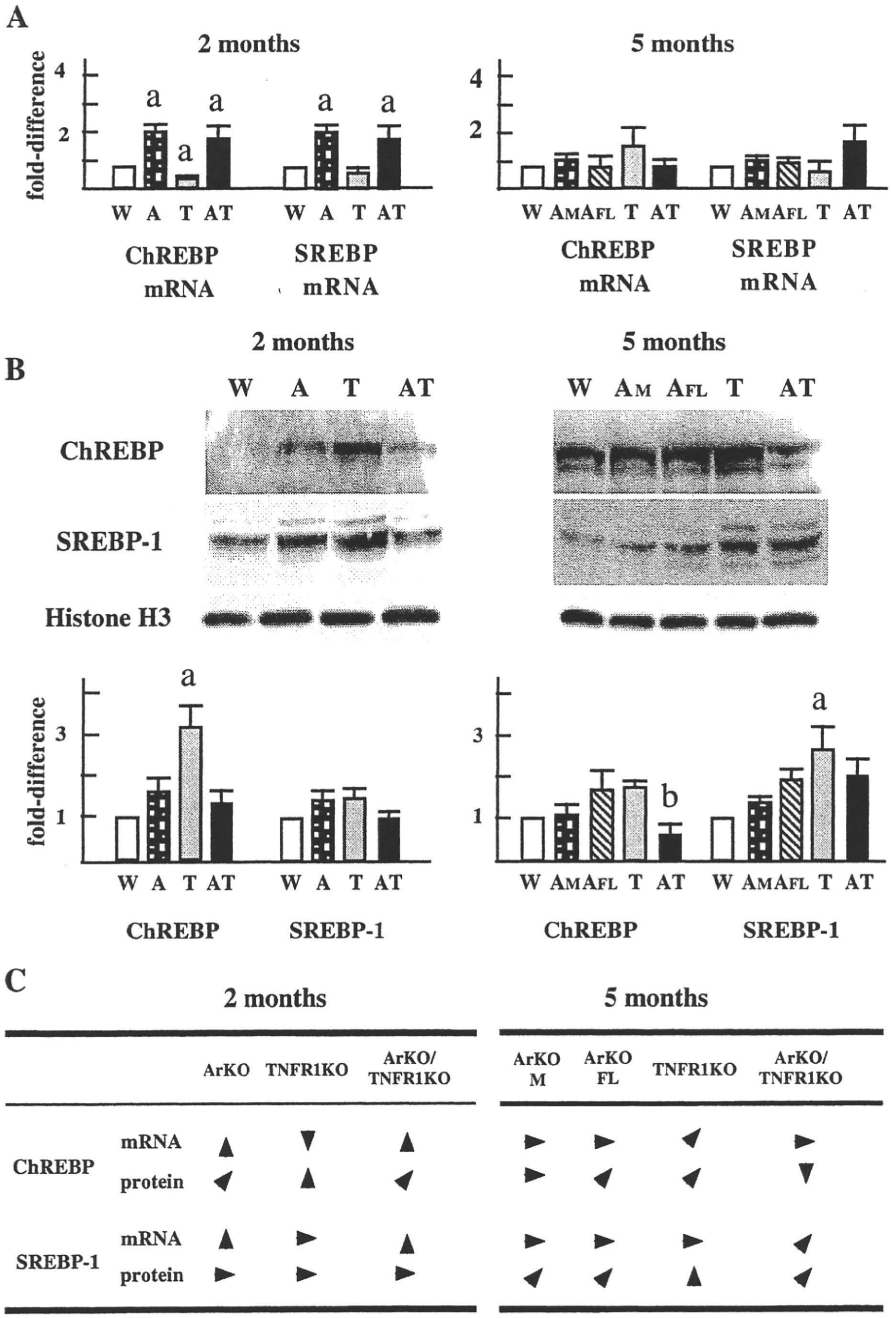

Fig. 6. Expression analysis of ChREBP and SREBP-1 in the livers. (A) Total RNA was extracted from livers of WT (W), ArKO (A, A_M, A_{FL}), TNFR1KO (T), and ArKO/TNFR1KO (AT) mice at 2 and 5 months of age. A_M and A_{FL} indicate ArKO mice that developed minimal and severe hepatic steatosis, respectively. Expression of mRNA for ChREBP and SREBP-1c were analyzed by real-time quantitative PCR, using primers described in the Materials and methods section. Results are presented as the mean ± SEM, $n = 5$/genotype. (a, $p < 0.05$, vs. WT mice). Results were normalized to cyclophilin mRNA values. (B) Immunoblot analysis of ChREBP and SREBP-1 protein in hepatic nuclear extracts. Nuclear extracts were prepared from livers of mice at 2 and 5 months of age. ChREBP (95 kDa) and SREBP-1 (68 kDa) proteins were detected, respectively, with ChREBP and SREBP-1 polyclonal antibodies. Histone H3 (16 kDa) polyclonal antibody was used as loading controls to normalize the signal obtained. (a, $p < 0.05$, vs. WT mice, and b, $p < 0.05$, vs. ArKO mice, $n = 6$/group). Representative immunoblot images are shown. (C) Summary of the analysis. The mRNA and protein respectively indicate results from QRT-PCR analysis of total RNA and immunoblot analysis of nuclear extracts. Horizontal arrowheads, upward arrowheads, arrowheads pointing up, downward arrowheads respectively indicate no changes, increases, increases without statistical significance and decreases as compared to the expression levels of WT mice.

In the present study, we measured the expression levels of ChREBP and SREBP-1; both are transcription factors contributing to the high rate of lipogenesis in liver [29]. Expression of mRNAs for both factors was significantly elevated in ArKO and ArKO/TNFR1KO mice at 2 months of age. Nevertheless, the elevated gene expression did not clearly reflect in their nuclear contents. Inconsistencies in mRNA and nuclear protein contents of ChREBP were also observed in TNFR1KO mice at 2 months of age, where mRNA for the factor was expressed at significantly lower levels than that in the WT mice, while its nuclear protein content was elevated. These observations thus support the fact that post-transcriptional regulation on ChREBP and SREBP-1 is important for controlling their nuclear actions [30] under the estrogen-deficient conditions as well. The nuclear ChREBP and SREBP-1 protein contents in the liver of ArKO mice that developed severe hepatic steatosis were not significantly different from those in ArKO mice with minimal steatosis. Expression of mRNA for Fasn and

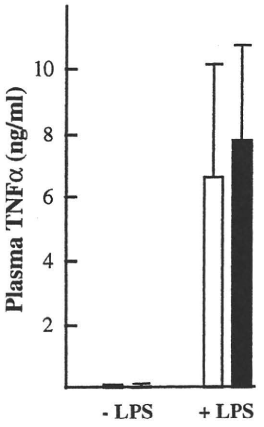

Fig. 7. TNF-α release in WT and ArKO mice after the injection of LPS. WT (open bar) and ArKO (closed bar) mice at 5 months of age were injected saline alone (−LPS) or LPS (10 ng/g of body weight) (+LPS). Plasma were prepared 1 h after the injection and used for the determination of TNF-α concentrations. Each value represents the mean ± SEM of five mice for LPS treatment and of seven mice for saline treatment.

Acaca genes, which are targets of SREBP-1 and involved in lipogenesis, was, however, induced less markedly in the former mouse models when compared to the latter. Furthermore nuclear protein contents of ChREBP in ArKO/TNFR1KO mice was significantly lower than that in the WT mice, while the former developed severe steatosis. These observations therefore suggest that nuclear protein levels of ChREBP and SREBP-1 might not necessarily associate with elevated expression of genes related to fatty-acid synthesis in the current animal models. Transcriptional activities of ChREBP and SREBP-1 are proposed to require cooperation with other nuclear factors to be functional [29]. Thus further studies including a specific technique to identify interacting factors or to inhibit hepatic expression of ChREBP and/or SREBP-1 genes are required to establish their exact roles in hepatic accumulation of lipid under estrogen-deficient conditions.

Adipose tissue-derived hormones such as adiponectin and leptin play important roles [31]; the former is known to be regulated reciprocally by TNF-α. However, in the current study, equivalent levels of plasma adiponectin were detected among the ArKO, ArKO/TNFR1KO, and WT mice, indicating that impairment in adiponectin production is not a major cause of the development of obesity in estrogen-deficient animal models in the regulation of whole-body energy homeostasis; nevertheless, it remains to be examined whether signaling systems that act through adiponectin receptors function properly under estrogen-deficient conditions. We did not detect a positive correlation between food-intake and the development of hepatic steatosis. Furthermore, serum leptin levels were elevated 2- to 3-fold in ArKO and ArKO/TNFR1KO mice compared to the levels in WT mice at 5 months of age, consistent with the previous reports [32,33]. The development of leptin-resistant phenotypes in estrogen-deficiency was also documented in mice lacking the ER-α gene [34].

The relevance of the estrogen functions in lipid metabolism in humans is suggested by patients with estrogen-signaling deficiency: a patient with an ER-α deficiency who showed glucose intolerance and hyperinsulinemia [35] and men with an aromatase gene mutation showing hyperinsulinemia [36]. Furthermore, the decline in estrogen function with the menopause is well recognized to be associated with spontaneous increases in serum proinflammatory cytokines including TNF-α, which might be the cause of the development of menopause-associated disorders such as bone loss, disturbance of vascular homeostasis, and atherosclerosis [37]. Thus, further studies on the interactions between regulatory systems mediated by estrogen and TNF-α are necessary to help the development of methods for the prevention and treatment of disorders in postmenopausal women.

Acknowledgements

This research was supported by a grant-in-aid for Scientific Research from the Ministry of Education, Culture, Sports, Science, and Technology of Japan (TS (c)21590849).

References

[1] P. Dandona, A. Aljada, A. Bandyopadhyay, Inflammation: the link between insulin resistance, obesity and diabetes, Trends Immunol. 25 (2004) 4–7.
[2] G.S. Hotamisligil, Inflammation and metabolic disorders, Nature 444 (2006) 860–867.
[3] G.S. Hotamisligil, The role of TNFα and TNF receptors in obesity and insulin resistance, J. Intern. Med. 245 (1999) 621–625.
[4] K.T. Uysal, S.M. Wiesbrock, M.W. Marino, G.S. Hotamisligil, Protection from obesity-induced insulin resistance in mice lacking TNF-alpha function, Nature 389 (1997) 610–614.
[5] M. Ryden, A. Dicker, V. van Harmelen, H. Hauner, M. Brunnberg, L. Perbeck, F. Lonnqvist, P. Arner, Mapping of early signaling events in tumor necrosis factor-α-mediated lipolysis in human fat cells, J. Biol. Chem. 277 (2002) 1085–1091.
[6] H. Ruan, H.F. Lodish, Insulin resistance in adipose tissue: direct and indirect effects of tumor necrosis factor-α, Cytokine Growth Factor Rev. 14 (2003) 447–455.
[7] A.T. Cheung, D. Ree, J.K. Kolls, J. Fuselier, D.H. Coy, M. Bryer-Ash, An in vivo model for elucidation of the mechanism of tumor necrosis factor-alpha (TNF-α) induced insulin resistance: evidence for differential regulation of insulin signaling by TNF-alpha, Endocrinology 139 (1998) 4928–4935.
[8] M. Saghizadeh, J.M. Ong, W.T. Garvey, R.R. Henry, P.A. Kern, The expression of TNF alpha by human muscle. Relationship to insulin resistance, J. Clin. Invest. 97 (1996) 1111–1116.
[9] P. Dandona, R. Weinstock, K. Thusu, E. Abdel-Rahman, A. Aljada, T. Wadden, Tumor necrosis factor-α in sera in obese patients: fall with weight loss, J. Clin. Endocrinol. Metab. 83 (1998) 2907–2910.
[10] Y. Nemoto, K. Toda, M. Ono, K.F. Adachi, T. Saibara, S. Onishi, H. Enzan, T. Okada, Y. Shizuta, Altered expression of fatty acid–metabolizing enzymes in aromatase-deficient mice, J. Clin. Invest. 105 (2000) 1819–1825.
[11] K.N. Hewitt, K. Pratis, M.E. Jones, E.R. Simpson, Estrogen replacement reverses the hepatic steatosis phenotype in the male aromatase knockout mouse, Endocrinology 145 (2004) 1842–1848.
[12] P.A. Heine, J.A. Taylor, G.A. Iwamoto, D.B. Lubahn, P.S. Cooke, Increased adipose tissue in male and female estrogen receptor-α knockout mice, Proc. Natl. Acad. Sci. U.S.A. 97 (2000) 12729–12734.
[13] C. Ohlsson, N. Hellberg, P. Parini, O. Vidal, M. Bohlooly-Y, M. Rudling, M.K. Lindberg, M. Warner, B. Angelin, J.A. Gustafsson, Obesity and disturbed lipoprotein profile in estrogen receptor-α-deficient male mice, Biochem. Biophys. Res. Commun. 278 (2000) 640–645.
[14] S.E. Bulun, I.M. Rosenthal, A.M. Brodie, S.E. Inkster, W.P. Zeller, A.M. DiGeorge, S.D. Frasier, M.W. Kilgore, E.R. Simpson, Use of tissue-specific promoters in the regulation of aromatase cytochrome P450 gene expression in human testicular and ovarian sex cord tumors, as well as in normal fetal and adult gonads, J. Clin. Endocrinol. Metab. 78 (1994) 1616–1621.
[15] K. Takeda, K. Toda, T. Saibara, M. Nakagawa, K. Saika, S. Onishi, T. Sugiura, Y. Shizuta, Progressive development of insulin resistance phenotype in male mice with complete aromatase (CYP19) deficiency, J. Endocrinol. 176 (2003) 237–246.
[16] K. Toda, K. Takeda, T. Okada, S. Akira, T. Saibara, T. Kaname, K. Yamamura, S. Onishi, Y. Shizuta, Targeted disruption of the aromatase P450 gene (Cyp19) in mice and their ovarian and uterine responses to 17β-oestradiol, J. Endocrinol. 170 (2001) 99–111.
[17] K. Toda, T. Okada, Y. Hayashi, T. Saibara, Preserved tissue structure of efferent ductules in aromatase deficient mice, J. Endocrinol. 199 (2008) 137–146.
[18] J.J. Peschon, D.S. Torrance, K.L. Stocking, M.B. Glaccum, C. Otten, C.R. Willis, K. Charrier, P.J. Morrissey, C.B. Ware, K.M. Mohler, TNF receptor-deficient mice reveal divergent roles for p55 and p75 in several models of inflammation, J. Immunol. 160 (1998) 943–952.
[19] D.S. Zarlenga, H.R. Gamble, Simultaneous isolation of preparative amounts of RNA and DNA from *Trichinella spiralis* by cesium trifluoroacetate isopycnic centrifugation, Anal. Biochem. 162 (1987) 569–574.
[20] R. Dentin, J.-P. Pe´gorier, F. Benhamed, F. Foufelle, P. Ferre, V. Fauveau, M.A. Magnuson, J. Girard, C. Postic, Hepatic glucokinase is required for the synergistic action of ChREBP and SREBP-1c on glycolytic and lipogenic gene expression, J. Biol. Chem. 279 (2004) 20314–20326.
[21] C. Le May, K. Chu, M. Hu, C.S. Ortega, E.R. Simpson, K.S. Korach, M.J. Tsai, F. M-Jarvis, Estrogens protect pancreatic β-cells from apoptosis and prevent insulin-deficient diabetes mellitus in mice, Proc. Natl. Acad. Sci. U.S.A. 103 (2006) 9232–9237.
[22] J.R. Bradley, TNF-mediated inflammatory disease, J. Pathol. 214 (2008) 149–160.
[23] G.S. Hotamisligil, A. Budavari, D. Murray, B.M. Spiegelman, Reduced tyrosine kinase activity of the insulin receptor in obesity-diabetes. Central role of tumor necrosis factor-alpha, J. Clin. Invest. 94 (1994) 1543–1549.
[24] B. Qin, R.A. Anderson, K. Adeli, Tumor necrosis factor-α directly stimulates the overproduction of hepatic apolipoprotein B100-containing VLDL via impairment of hepatic insulin signaling, Am. J. Physiol. Gastrointest. Liver Physiol. 294 (2008) G1120–G1129.
[25] S.A. Schreyer, S.C. Chua Jr, R.C. LeBoeuf, Obesity and diabetes in TNF-alpha receptor-deficient mice, J. Clin. Invest. 102 (1998) 402–411.
[26] M. Monetti, M.C. Levin, M.J. Watt, M.P. Sajan, S. Marmor, B.K. Hubbard, R.D. Stevens, J.R. Bain, C.B. Newgard, R.V. Farese Sr, A.L. Hevener, R.V. Farese Jr,

Dissociation of hepatic steatosis and insulin resistance in mice overexpressing DGAT in the liver, Cell Metab. 6 (2007) 69–78.
[27] C. Postic, J. Girard, Contribution of de novo fatty acid synthesis to hepatic steatosis and insulin resistance: lessons from genetically engineered mice, J. Clin. Invest. 118 (2008) 829–838.
[28] T. Ota, C. Gayet, H.N. Ginsberg, Inhibition of apolipoprotein B100 secretion by lipid-induced hepatic endoplasmic reticulum stress in rodents, J. Clin. Invest. 118 (2008) 316–332.
[29] B. Desvergne, L. Michalik, W. Wahli, Transcriptional regulation of metabolism, Physiol. Rev. 86 (2006) 465–514.
[30] R. Dentin, J. Girard, C. Postic, Charbohydrate responsive element binding protein (ChREBP) and sterol regulatory element binding protein-1c (SREBP-1c); two key regulators of glucose metabolism and lipid synthesis in liver, Biochimie 87 (2005) 81–86.
[31] T. Kadowaki, T. Yamauchi, Adiponectin and adiponectin receptors, Endocr. Rev. 26 (2005) 439–451.
[32] M.E. Jones, A.W. Thorburn, K.L. Britt, K.N. Hewitt, N.G. Wreford, J. Proietto, O.K. Oz, B.J. Leury, K.M. Robertson, S. Yao, E.R. Simpson, Aromatase-deficient (ArKO) mice have a phenotype of increased adiposity, Proc. Natl. Acad. Sci. U.S.A. 97 (2000) 12735–12740.
[33] M.L. Misso, Y. Murata, W.C. Boon, M.E. Jones, K.L. Britt, E.R. Simpson, Cellular and molecular characterization of the adipose phenotype of the aromatase-deficient mouse, Endocrinology 144 (2003) 1474–1480.
[34] G. Bryzgalova, H. Gao, B. Ahren, J.R. Zierath, D. Galuska, T.L. Steiler, K. Dahlman-Wright, S. Nilsson, J.A. Gustafsson, S. Efendic, A. Khan, Evidence that oestrogen receptor-alpha plays an important role in the regulation of glucose homeostasis in mice: insulin sensitivity in the liver, Diabetologia 49 (2006) 588–597.
[35] E.P. Smith, J. Boyd, G.R. Frank, H. Takahashi, R.M. Cohen, B. Specker, T.C. William, D. B. Lubahn, K.S. Korach, Estrogen resistance caused by a mutation in the estrogen-receptor gene in a man, N. Engl. J. Med. 331 (1994) 1056–1061.
[36] L. Maffei, Y. Murata, V. Rochira, C. Aranada, M. Vasquez, G. Tubert, C.D. Clyne, E.R. Simpson, C. Carani, Dysmetabolic syndrome in a man with a novel mutation of the aromatase gene: effects of testosterone, alendronate and estradiol treatment, J. Clin. Endocrinol. Metab. 89 (2004) 61–70.
[37] J. Pfeilschifter, R. Köditz, M. Pfohl, H. Schatz, Changes in proinflammatory cytokine activity after menopause, Endocr. Rev. 23 (2002) 90–119.

JPP Journal of Pharmacy and Pharmacology

JPP 2010, 62: 241–246

Received May 15, 2009
Accepted November 10, 2009
DOI 10.1211/jpp/62.02.0012
ISSN 0022-3573

Research Paper

Effects of *Eriobotrya japonica* seed extract on oxidative stress in rats with non-alcoholic steatohepatitis

Saburo Yoshioka[a], Atsuhide Hamada[a], Kohei Jobu[a], Junko Yokota[a], Masahide Onogawa[a], Shojiro Kyotani[a], Mitsuhiko Miyamura[a], Toshiji Saibara[b], Saburo Onishi[b] and Yutaka Nishioka[a]

Departments of [a]Pharmacy and [b]Gastroenterology and Hepatology, Kochi Medical School, Nankoku, Kochi, Japan

Abstract

Objectives Non-alcoholic steatohepatitis is associated with the deposition of lipid droplets in the liver, and is characterised histologically by the infiltration of inflammatory cells, hepatocellular degeneration and liver fibrosis. Oxidative stress may play an important role in the onset and deterioration of non-alcoholic steatohepatitis. We previously reported that an *Eriobotrya japonica* seed extract, extracted in 70% ethanol, exhibited antioxidant actions *in vitro* and *in vivo*. In this study, we examined the effect of this extract in a rat model of non-alcoholic steatohepatitis.

Methods The seed extract was given in the drinking water to fats being fed a methionine-choline-deficient diet for 15 weeks.

Key findings Increases in alanine aminotransferase and aspartate aminotransferase levels were significantly inhibited in rats fed the seed extract compared with the group on the diet alone. Formation of fatty droplets in the liver was also inhibited. Antioxidant enzyme activity in liver tissue was higher than in the diet-only group and lipid peroxidation was reduced compared with rats that also received the extract. Expression of 8-hydroxy-2′-deoxyguanosine and 4-hydroxy-2-nonenal was lower in the rats given the seed extract than in the diet-only group. In the former, liver tissue levels of transforming growth factor-β and collagen were also decreased.

Conclusions Thus, the *E. japonica* seed extract inhibited fatty liver, inflammation and fibrosis, suggesting its usefulness in the treatment of non-alcoholic steatohepatitis.

Keywords antioxidant enzyme activity; *Eriobotrya japonica* seed extract; non-alcoholic steatohepatitis; oxidative stress; methionine-choline-deficient diet

Introduction

In 1980, Ludwig and colleagues described a patient with no history of alcohol abuse but in whom liver biopsy showed histological features similar to alcoholic injury.[1] Since then, non-alcoholic steatohepatitis (NASH) has been investigated extensively. NASH is defined as steatosis with inflammation and fibrosis, excluding many liver disorders such as viral hepatitis. In some patients, it deteriorates to liver cirrhosis, leading to the development of hepatocellular carcinoma.[2–4] The pathogenesis of this disorder may initially involve fatty changes in hepatocytes, oxidative stress, insulin resistance, dyslipidaemia, excessive iron deposition and mitochondrial dysfunction.[5] As a factor involved in the deterioration of NASH, oxidative stress may be associated with reactive oxygen species (ROS) synthesised by the excessive amount of adipose tissue-derived free fatty acids when oxidised by mitochondria and cytochrome P450 2E1 (CYP2E1), the production of inflammatory cytokines, such as tumour necrosis factor-α and transforming growth factor-β (TGF-β), and the Fenton reaction of iron deposition in the liver.[6]

The treatment of NASH involves diet/exercise therapies,[7] insulin-sensitising agents,[8] ursodeoxycholic acid[9] and fibrate lipid-lowering agents.[10] Recent studies indicated that angiotensin II receptor blockers reduced liver fibrosis in the presence of NASH.[11,12] However, appropriate treatment has not been established.

Eriobotrya japonica seed extract (ESE) is a health food with antioxidative activity. It exhibits radical scavenging activity against ROS such as superoxide anion, hydrogen

Correspondence: Saburo Yoshioka, Department of Pharmacy, Kochi Medical School Hospital, Oko-cho, Nankoku, Kochi 783-8505, Japan.
E-mail: jm-saburo@kochi-u.ac.jp

peroxide, hydroxyl radicals and lipid peroxide (LPO).[13] We have previously shown, using HPLC, that this extract contains various substances such as polyphenols (caffeic and chlorogenic acids), amino acids and unsaturated fatty acids.[14,15] Multiple components of ESE are considered to act additively or synergistically, showing direct antioxidant and biological regulatory actions. To date, we have reported the usefulness of ESE in the treatment of various disorders in which oxidative stress is aetiologically involved, such as nephropathy,[16] mucositis,[14] adverse reactions to anticancer agents, gastric mucosal injury related to non-steroidal anti-inflammatory drugs[15] and allergy reactions.[17,18] Furthermore, ESE decreased the level of low-density lipoprotein cholesterol in rabbits with hyperlipidaemia.[19]

According to a recent study, the histopathology of liver biopsies from rats fed a methionine-choline-deficient (MCD) diet resembles those in NASH. In this study, we administered ESE, which was extracted by 70% ethanol, to a model of NASH in rats fed an MCD diet.

Materials and Methods

Materials

Sufficiently sun-dried seeds of Mogi-loquant collected in Muroto and Susaki Cities in Kochi Prefecture and Shimotsu-cho in Wakayama Prefecture, Japan, were used. All other chemicals were of reagent grade.

Extraction of seeds

E. japonica seeds were extracted in 70% ethanol. Briefly, 1.0 kg of seeds were crushed in a refrigerated blender at 1000 rev/min, and then stirred continuously by a mixer at 300 rev/min for 7 days after being dissolved in 70% ethanol. The supernatant was then collected and evaporated to dryness. The final yield of the extract was about 120 g. The dried extract was emulsified in 6.6 litres distilled water.

The extract was made in large quantities in this ratio and the same batch has been used for various studies since 2008.[18]

Animals

Male Wistar rats (aged 5 weeks and weighing 90–110 g) were purchased from Japan SLC, Inc. (Shizuoka, Japan) and were acclimatised for 7 days at 23 ± 2°C with free access to a normal diet (CE-2, Clea, Osaka, Japan) and water. Healthy rats were then selected and randomly divided into three groups. Rats were fed either the MCD diet (Oriental Yeast, Tokyo, Japan) or a normal diet. Three experimental groups were studied. The normal group ($n = 6$) was fed a standard diet and received water *ad libitum*. The other two groups ($n = 7$) were fed the MCD diet and water. One of these groups were also given ESE in conjunction with the MCD diet (0.27 g/day in drinking water, using a water-supply bottle at a dose of 15 ml/day). It was confirmed that the rats consumed the treated water each time. All rats were fed for 15 weeks under these conditions.

All animal experiments were performed according to the guidelines for the care and use of laboratory animals of Kochi University, and were approved by our local ethics committee for experimental animal use.

Tissue preparation

At the end of the treatment period, the rats were fasted overnight, anaesthetised with pentobarbital (50 mg/kg), and blood and liver samples taken. The liver samples were perfused *in situ* with cold phosphate-buffered saline to remove circulating blood cells. Each sample (approximately 0.4 g) was weighed and then homogenised with a cell homogeniser (Polytron PT3100, Kinematica AG, Lucerne, Germany) in an extraction buffer containing 20 mmol/l Tris-HCl, pH 7.5, 2 mol/l NaCl, 0.1% Tween 80, 1 mmol/l EDTA and 1 mmol/l phenylmethylsulfonyl-fluoride. Supernatants obtained after centrifugation at 15 000*g* for 30 min at 4°C were stored at −70°C.

Measurement of liver enzymes and markers

Plasma samples were obtained immediately by centrifuging blood samples at 3000 rev/min for 10 min. Plasma aspartate aminotransferase (AST) and alanine aminotransferase (ALT) activities were measured using a Fuji Dri-Chem analyser (Fujifilm Medical Co., Ltd, Tokyo, Japan).

Superoxide dismutase (SOD) in liver tissue was measured using a commercial kit (Dojindo Laboratories, Kumamoto, Japan). Glutathione peroxidase (GPx) and catalase activities were measured using commercial kits from Cayman Chemical Co. (Ann Arbor, MI, USA).

Levels of glutathione (GSH) in liver tissue were measured using an assay kit from Cayman Chemical Co. LPO was measured using a test kit from Wako Pure Chemical Industries (Osaka, Japan). TGF-β was measured by immunoassay using a commercial kit (Multispecies TGF-β1; BioSource Int., Camarillo, CA, USA). Collagen levels were measured using a staining kit (MCK, Tokyo, Japan).

Histopathology and immunohistochemistry

Immediately after removal, livers were fixed in 10% formalin for 48 h, and then embedded in paraffin. Sections 5 μm thick were then routinely processed for staining with haematoxylin and eosin (H&E) and Azan.

For immunohistochemical analysis, Histofine Simple Stain Rat MAX PO (Nichirei Biosciences, Tokyo, Japan) was used in combination with anti-8-hydroxy-2′-deoxy-guanosine (8-OHdG), 5 μg/ml, and anti-4-hydroxy-2-nonenal

Table 1 Effect of *E. japonica* seed extract (ESE) on body weight and liver enzymes after 15 weeks

	Normal	MCD diet	MCD diet + ESE
Body weight (g)	307.3 ± 9.2	79.7 ± 0.6**	86.9 ± 1.5
ALT (U/l)	51.0 ± 4.9	160.0 ± 11.9**	103.0 ± 16.7†
AST (U/l)	91.5 ± 10.2	154.6 ± 23.3*	95.8 ± 8.1†

Values are means ± SEM (n = 5–7 experiments). $^{*}P < 0.05$; $^{**}P < 0.01$ vs normal group; $^{\dagger}P < 0.05$ vs MCD diet group (Tukey–Kramer's test). ALT, alanine aminotransferase; AST, aspartate aminotransferase; MCD, methionine-choline-deficient.

(4-HNE), 5 μg/ml (both Oxis International, Beverly Hills, CA, USA).

Statistical analysis

Data are given as means ± SEM. The level of statistical significance was determined by analysis of variance followed by Tukey–Kramer's test for multiple comparisons. P values less than 0.05 were considered significant.

Results

Effect of ESE on body weight, ALT and AST

The body weight and plasma levels of ALT and AST after 15 weeks are shown in Table 1. Body weight at week 15 was significantly lower in the diet group than in the normal group ($P < 0.01$) but was higher in the diet/ESE group than in the diet group. Plasma ALT and AST levels were significantly higher in the diet group than the normal group ($P < 0.01$ and

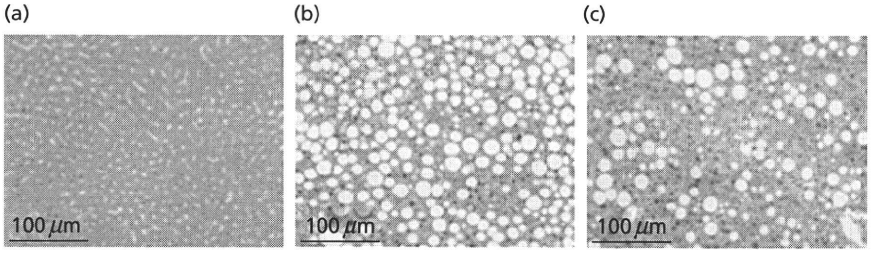

Figure 1 Effect of *E. japonica* seed extract (ESE) on diet-related fatty liver. Samples were taken from rats fed (a) a normal diet, (b) a methionine-choline-deficient (MCD) diet or (c) the MCD diet with ESE in the drinking water. Samples from rats fed the normal diet show normal hepatocytes. Samples from rats fed the MCD diet show diffuse macrosteatosis and hepatocellular ballooning. Samples from the rats fed ESE and the MCD diet show reduction in steatosis. Samples are stained with haematoxylin and eosin.

Table 2 Effect of *E. japonica* seed extract (ESE) on oxidative stress in liver tissue after 15 weeks

	Normal	MCD diet	MCD diet + ESE
SOD (U/mg protein)	332.4 ± 17.7	193.8 ± 15.1*	308.1 ± 49.0†
GPx (μmol/min per mg protein)	1315.5 ± 60.1	344.5 ± 40.1**	532.5 ± 51.5†
Catalase (μmol/min per mg protein)	2.96 ± 0.38	1.60 ± 0.14**	1.64 ± 0.06
GSH (nmol/mg protein)	186.8 ± 13.0	138.7 ± 8.4*	184.3 ± 12.0†
LPO (nmol/mg protein)	63.9 ± 4.2	126.7 ± 17.4**	73.0 ± 4.4‡

Values are means ± SEM (n = 4–6 experiments). $^{*}P < 0.05$; $^{**}P < 0.01$ vs normal group; $^{\dagger}P < 0.05$, $^{\ddagger}P < 0.01$ vs MCD diet group (Tukey–Kramer's test). GPx, glutathione peroxidase; GSH, glutathione; LPO, lipid peroxide; MCD, methionine-choline-deficient; SOD, superoxide dismutase.

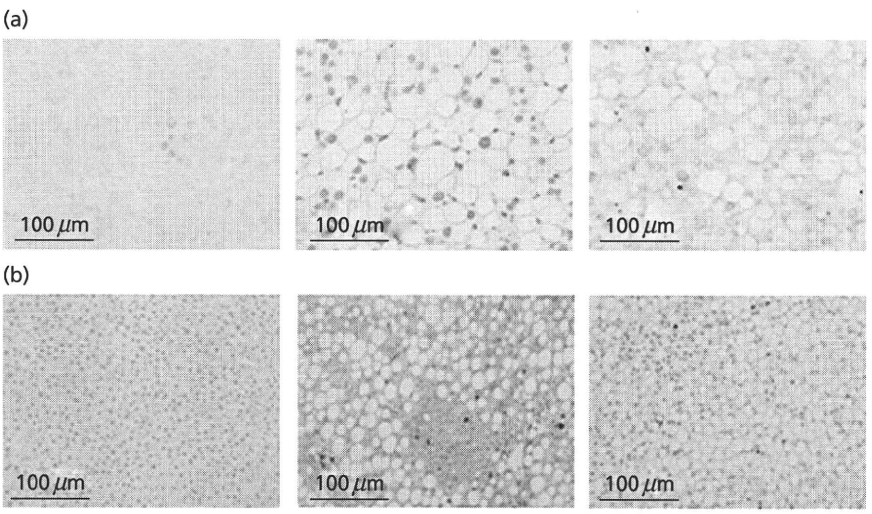

Figure 2 Effect of *E. japonica* seed extract (ESE) on expression of (a) 8-hydroxy-2′-deoxyguanosine (8-OHdG) and (b) 4-hydroxy-2-nonenal (4-HNE). Representative livers from rats fed a normal diet (left), methionine-choline-deficient (MCD) diet (centre) or MCD diet with ESE in the drinking water (right). In (a), 8-OHdG positive cells are identified by the brown nuclei in the photomicrographs. In (b) 4-HNE positive cells are identified by the brown cytoplasm in the photomicrographs.